

**Examining forest structure in the Mozambican Dry Deciduous Lowland Forest
utilizing in-situ and remotely sensed measurements and observations**

Ethan Koesters Heil
Salem, Virginia

B.S. Civil Engineering, University of Virginia, 2011

A Thesis presented to the Graduate Faculty
of the University of Virginia in Candidacy for the Degree of
Master of Science

Department of Environmental Science

University of Virginia
August, 2013

Abstract

Land use change in the form of deforestation and degradation is contributing to the release of greenhouse gases on the order of 1.2 ± 0.7 Gt CO₂e per year. Emissions of this magnitude suggest that the conversion and disturbance of forests play a significant role in forcing global climate change. Although there is growing recognition of this contribution among scientific and political communities, there is an expressed need for more efficient and accurate methods for assessing the role of forests in shifting climate patterns. Recent efforts to measure and monitor forests on large scales have used remotely sensed data from airborne and spaceborne sensors. This study leverages high spatial resolution remotely sensed data with in-situ field measurements to measure forest structure in the Dry Deciduous Lowland Forests of Mozambique. The approach to analysis was motivated by the importance of three-dimensional forest structure in driving forest dynamics. A novel tree crown analysis methodology was employed in order to calculate select structural properties of forests from remotely sensed data. The results of this analysis were not deemed accurate enough to be considered robust geophysical measurements. However, the study provides a step forward in the application of this methodology to the classification of terrestrial surfaces and to the detection of forest degradation due to anthropogenic lumber harvesting disturbance.

Table of Contents

Abstract	0
1 Introduction.....	3
1.1 Forests as part of a global system.....	3
1.2 Tropical forests, deforestation and land use change	5
1.3 The role of remote sensing	6
1.4 Importance of forest structure	8
1.5 Remote sensing of forest structure	10
1.5.1 Fine-scale passive remote sensing	12
1.5.2 Medium-scale passive remote sensing.....	13
1.5.3 Coarse-scale passive remote sensing	14
1.5.4 Active remote sensing.....	15
1.6 Dry tropical forests	18
1.7 Forest use in the Sofala Province of Mozambique	19
2 Project Description.....	21
2.1 Research Hypotheses	21
2.2 Study Area.....	21
3 Methods	27
3.1 Field data acquisition	29
3.2 Remote sensing data acquisition	35
3.3 Field data processing	38
3.4 Remote sensing data preprocessing	41
3.5 Remote sensing analysis	43
3.5.1 Software calibration.....	45
3.5.2 Software analysis	55
3.5.3 Results postprocessing	58
3.6 Numerical analysis.....	60
3.7 Comparative analysis	61
4 Results	62
5 Discussion and Significance	81
5.1 Supplemental Research Suggestions	84
6 Acknowledgements	86
7 Bibliography	89
8 Appendices	99
8.1 Appendix A	99
8.2 Appendix B	101
8.3 Appendix C	102

1 Introduction

1.1 Forests as part of a global system

Forests play a unique and dynamic role in a complex global system. These unique ecosystems provide a vast array of essential functions as part of broader environmental, social, economic and political systems. Forest ecosystems are often viewed in terms of the tangible environmental goods and services they provide, which can subsequently be divided into timber or non-timber concerns. Timber products are explicitly associated with forests, and refer to lumber and other goods (such as paper) which trace their material roots back to trees. Services provided by the consumption of timber range from the localized heating provided by small campfires to the electricity provided by industrial-scale wood pellet-based power plants. Forest ecosystems also provide countless non-timber (and often less obvious) goods and services ranging from habitat preservation and shelter to nutrient and chemical cycling. While the benefits of forests are numerous, in certain forested areas, economic, social and political pressures are contributing to unsustainably extractive and destructive practices. Meanwhile, increasing recognition of the broad, essential roles of forests is contributing to concerns over the potential long-term negative consequences associated with these actions.

In light of growing concerns regarding the role of greenhouse gases in forcing global climate change, understanding the movement of carbon through forest ecosystems is becoming increasingly important. The link between forests and climate change forcing is compelling with as much as 12-20% of global anthropogenic carbon emissions resulting from deforestation and land use change (Le Quere, et al., 2009). Essentially, these emissions come from the conversion of carbon stocks as a sequestered form of vegetative biomass into greenhouse gases such as

carbon dioxide and methane. To better understand and manage the carbon balance of terrestrial ecosystems, more information is needed about how biomass is being released in the form of atmospheric greenhouse gases and how these emissions can be mitigated. Efforts at quantifying carbon emissions due to deforestation and land use change are still evolving and lacking in empirical rigor (Houghton, 2003; Corbera, Estrada, & Brown, 2010). This is illustrated by significantly larger percentage uncertainty associated with greenhouse gas emissions due to deforestation (1.2 ± 0.7 Gt CO₂e/a) as compared to those due to fossil fuel use (8.7 ± 0.5 Gt CO₂e/a). Additionally, an imbalance in the global carbon budget has led to speculations of a 1.6 Gt C/a unidentified terrestrial sink (Forster, 2007). Ideally, the application of new and more expansive methods for measuring carbon cycling in terrestrial ecosystems will lead to a reduction in this uncertainty and inform attempts to reduce future emissions.

The emergence of new methodologies (including those utilizing remote sensing techniques) for measuring and monitoring forest ecosystems coincides with greater awareness of global climate change and other large-scale, human-induced ecological shifts. As such, there is a broad-based social, economic, political and scientific movement to leverage these methods to enhance understanding of the role of forests and learn how to manage them in a sustainable, mutually beneficial manner. The aim of this research is to contribute incrementally to this much larger movement by examining forest structure in a relatively understudied area in the Dry Deciduous Lowland Forests of Mozambique. Accordingly, this research intends to develop and employ a suitable methodology for measuring forest structural properties using a combination of in-situ data collection and high resolution remote sensing analysis. This will in turn allow for a comparative analysis of forest structure among sites that experience varying degrees of anthropogenic forest disturbance, including: preserved forests, community-use forests,

traditionally extractive commercial logging operations, and an innovative, sustainable use forestry.

1.2 Tropical forests, deforestation and land use change

Land use change, particularly in the context of deforestation, refers to the intentional removal of forests. For thousands of years, land use change has been driven by the desire to increase arable or pastoral agricultural land and make room for settlement. Deforestation also comes from resource extraction, wherein trees or other vegetation are removed in a manner that alters the original forest ecosystem. Degradation refers to less visible forest disturbances in the form of selective logging or understory livestock grazing. The result of deforestation and degradation is the disruption of natural forest processes with broad ranging implications that can take decades or centuries to recover. Among the most significant effects of deforestation and degradation, is the release of greenhouse gases. As forests are cleared or disrupted, sequestered carbon within terrestrial biomass and soil is released through decomposition, fire, tilling and other anthropogenic activities (Geist & Lambin, 2002; Boucher, et al., 2011; DeFries, Rudel, Uriarte, & Hansen, 2010). As previously noted, up to one fifth of all anthropogenic greenhouse gas emissions are due to land conversion practices and deforestation. Additional climate forcing affects associated these practices include the alteration of albedos by changing the reflectance characteristics of landscapes and introducing black carbon to the atmosphere through burning (Hely, Caylor, Alleaume, Swap, & Shugart, 2003; Kuhlbusch, et al., 2012).

Although land-use changes are occurring on a global scale, about 60% of the carbon dioxide emissions from these activities occur in the form of deforestation within the tropics (Houghton, 2003; Hansen, Stehman, & Potapov, 2010; Achard, et al., 2002). Various

international private and governmental organizations have recognized the significance of this source of greenhouse gases and have attempted to incentivize the protection of tropical forests in order to reduce emissions. These efforts have progressed in tandem with the promotion of corollary benefits such as the preservation of biodiversity and watershed management. Programs such as the United Nations' Reducing Emissions from Deforestation and Forest Degradation (REDD+), the World Bank's Forest Carbon Partnership Facility (FCPF), and the Governors' Climate and Forests (GCF) Task Force have developed programs that provide financial incentives for the preservation of carbon stocks in tropical regions. While these programs take different approaches, a common concern is the difficulty associated with measuring and monitoring these carbon stocks (Governors' Climate and Forests Task Force, 2009; Food and Agriculture Organization of the United Nations, United Nations Development Program, United Nations Environment Programme, 2008; Gordon, Tam, Bosquet, & Aquino, 2011).

The reasons behind the aforementioned trends in deforestation and land use change are complex, and are subject to a variety of political, social, economic and environmental influences. For many, forested lands are viewed as a resource, whether as a potential field for pastoral grazing, a bank of harvestable timber or a preserve of biodiversity. Regardless of viewpoint, it is important to understand not only what role forests play in changing global systems, but also how they in turn respond to such changes.

1.3 The role of remote sensing

In order to best reduce, mitigate, and manage changes that may affect human society and the Earth as a whole, efforts need to be taken to understand how humans are altering the environment and what effects they are causing. Remote sensing applications are well-suited to

contribute to research on global climate change in various ways, ranging from measuring atmospheric and sea surface temperatures to monitoring changes in polar ice mass. Remote sensing techniques allow researchers to analyze data on spatial and temporal scales that are often orders of magnitude greater than those which could be similarly analyzed from an in-situ perspective. The development of techniques that provide observations of the Earth on global and decadal scales coincides opportunely with the growing recognition of global environmental issues.

Remote sensing techniques can additionally be used to observe and monitor terrestrial processes that dynamically interact with the global climate. In particular, there exists a promising array of remote sensing methods that can be employed to measure and monitor forests. While all of these techniques rely on measuring the forests' interaction with and reflection of electromagnetic radiation, a wide variety of variables and otherwise helpful metrics can be gathered through remote sensing. Some methodologies provide simple Boolean classification of forested versus non-forested areas, while others allow for measurement of actual geophysical values such as the fraction of Absorbed Photosynthetically Active Radiation (fAPAR) or crown geometry.

Some of the most common variables utilized in the remote sensing of forests are the Normalized Difference Vegetation Index (NDVI), Leaf Area Index (LAI) and the Enhanced Vegetation Index (EVI) (Adams & Gillespie, 2006). These measures represent simple ratios of electromagnetic reflection at different wavelengths, and are easily calculated and obtained from a wide variety of satellite payloads. Perhaps because of their ready availability and ease of calculation, many forest properties have been assessed using these ratio-based calculations. Despite their ease of use, these measures are empirically limited by their high level of

uncertainty. Because these parameters respond to changes unrelated to vegetation, such as soil moisture, atmospheric attenuation, sun positioning and anisotropy, there is a high level of measurement error which limits the correlation of these values with actual forest parameters, such as structure or productivity. In fact, NDVI was devised in the 1970's according to the data available at the time, not because it represented the most robust methodology for measuring forest properties (Myeni, 1993). As such, it is important to recognize the limitations of remotely sensed data and to make an attempt to provide supplemental data when applicable.

There are a growing number of terrestrial remote sensing techniques that provide various tradeoffs in terms of accuracy, spatial resolution, spatial extent, and temporal span. These methods, in turn, provide insight into a variety of forest characteristics, including changes due to anthropogenic degradation, productivity, phenology, senescence, biodiversity, and forest structure. This study uses methods for measuring forest structure and related properties, which are expounded in section 1.5.

1.4 Importance of forest structure

Remote sensing methods for monitoring and measuring forests are useful in quantifying the role of forests as part of broader societal issues, including climate change and biodiversity preservations. In order to frame forests within these contexts, several forest metrics have become increasingly important as part of global, transdisciplinary discussions. These include biomass and productivity measurements, which are crucial in understanding the flow and stores of carbon within forest ecosystems.

Forest biomass provides a measurement of sequestered carbon (in mass units) and includes organic matter in the form of above and below ground living vegetation (trees, shrubs,

saplings, vines, etc) as well as dead vegetation (leaf litter, downed logs, etc). Obtaining reasonable estimates for below ground biomass and dead vegetation is extremely difficult with current techniques, and is often time and cost prohibitive (Casper, Schenk, & Jackson, 2003; Hely, Caylor, Alleaume, Swap, & Shugart, 2003). As such, the majority of biomass estimates focus on above ground living biomass (AGB), which includes standing vegetation such as leaves, stems, branches, vines, trunk and bark. AGB is generally regarded as containing the majority of biomass within forests (though some particular trees have been shown to contain more below ground biomass than above ground) and is assumed to be a good proxy for total biomass (Brown, 1997). It should be noted that current measurements of biomass rarely take into account the significant quantities of carbon stored within the soil substrate.

Productivity measures assess the rates at which forests are fixing carbon (in mass units per area per time) through photosynthesis. Gross primary productivity (GPP) refers to the amount of total carbon captured through photosynthetic activities, while net primary productivity (NPP) is used more specifically to refer to the carbon that is converted into biomass (Field, Randerson, & Malmstrom, 1995). GPP and NPP are difficult to measure in-situ, but can be done using carbon flux towers, which measure the concentration of carbon within influent and effluent carbon eddies above the forest canopy (Burba & Anderson, 2010).

Given the role of carbon in the context of global climate change, it becomes clear why biomass and productivity are important variables. Unfortunately, the in-situ measurement of these variables is often prohibitively expensive and tedious. As such, efforts have been made to create algorithms that correlate remote sensing and empirical observations. While this seems like a promising approach, these methods do not allow for direct measurement of biomass or productivity and tend to rely on correlations and relationships among pixel reflectance values.

In recognition of such limitations, the National Research Council Committee on Earth Science and Applications from Space calls for the incorporation of forest structure into remote sensing analyses of forests as a top priority (Committee on Earth Science and Applications from Space: A Community Assessment and Strategy for the Future, 2007). Many current methodologies are limited by their reliance on a two dimensional conceptualization of forests. In the manner of form influencing function, the three dimensional structure of a forest plays a significant role in determining forest processes. The converse, which states function also influences form, highlights the notion that forest structure will in turn adapt as forest processes change. Incorporating the influence of horizontal and vertical forest structure in scientific studies will thus allow for a better understanding of forest dynamics. As such, measurements based on the inclusion of forest structure have the potential to greatly reduce uncertainty in measurements of forest biomass, carbon cycling, productivity, energy balance and even habitat diversity (Shugart, Saatchi, & Hall, 2010; Frohking, et al., 2009).

Forest structure can be discerned from a number of measurements and observations, including biomass, canopy geometry, tree architecture, distribution of tree sizes and tree density, among others (Spies, 1998). Recent advancement in high resolution passive, radar and LiDAR remote sensing technologies provide the tools to directly measure several of these properties, though each method has inherent benefits and limitations tied to resolution and scale (Shugart, Saatchi, & Hall, 2010).

1.5 Remote sensing of forest structure

Current methods for measuring forest structure generally fall into the following categories: field measurement methods, remote sensing methods, and geographic information

systems (GIS) methods (Lu, 2006). Each of these methods has their respective strengths and limitations. Field measurement-based methodologies of measuring structure are generally regarded as the most accurate, but require significant amounts of time, expertise, manpower and equipment - which all in turn translate to a prohibitive financial burden for monitoring anything other than small measurement plots. That being said, field-based measurement are often required in one form or another in order to calibrate, validate and/or verify observations using other techniques such the GIS-based or remote sensing-based approaches. GIS-based approaches have been used to some degree in the past because of the ease in obtaining the required inputs for this sort of inventory. GIS-based estimates rely on land cover classification maps that relate different types of land cover to different forest structure estimations. These estimates often do not require extensive expertise and monetary resources and allow underresourced, developing countries to self-report their land classification (Brown, 1997). While promoting national sovereignty, these methods are not standardized and are often riddled with uncertainty, inconsistency, and misclassification of land cover type (Grainger, 2008). This type of approach can often be seen as a derived method of the other two approaches, as the land cover classification maps that drive such an analysis are often created with data from field-based and remotely-sensed observations.

Remote sensing methods provide alternatives to some of the issues raised by field-based and GIS-based method, but there is currently no “best method” for remote sensing of forest structure. In fact, there are several types of approaches, each with their own respective strengths and weaknesses. They can be broken up into four broad categories including: fine spatial resolution (fine-scale) passive approaches, medium spatial resolution (medium-scale) passive approaches, coarse spatial resolution (coarse-scale) passive approaches, and active remote

sensing approaches. The nature of these different methods is such that there are tradeoffs in temporal and spatial resolution, availability and cost at each scale (Lu, 2006).

1.5.1 Fine-scale passive remote sensing

Fine spatial resolution (typically less than one meter) approaches to measuring forest structure using passive remote sensing sensors represent the method closest in scale to actual in-situ measurement, and thus tend to reflect the most accurate methods of any passive approach. Unfortunately, it also has similar limitations in terms of spatial extent and cost, as high resolution images often come from proprietary satellites (IKONOS, QuickBird) or aerial mounted cameras. Thus these images are not free of charge and it is often prohibitively expensive to acquire data for areas on the regional and national scale or at high temporal resolution. Another caveat includes the necessity to handle large quantities of data when analyzing these images. The particular strengths and limitations of fine-scale passive approaches tend to place these methods as intermediate analyses that are calibrated using field measurements, and are often extrapolated to larger scales in conjunction with medium or coarse-scale approaches (Gonzalez, et al., 2010; Hurtt, et al., 2003).

Many of the benefits of using fine-scale passive remote sensing techniques are due to the fact that the scale of the structural characteristic of interest is often larger than the resolution of the image. For this reason, the trees in an image can be individually delineated and measured. This is the basic approach that will be utilized in the proposed research. Typically, tree crowns are demarcated manually or automatically using algorithms that scan visible panchromatic or false color images (Broadbent, Asner, Pena-Claros, Palace, & Soriano, 2008). Palace et al. (2008) reveal that automated methods of tree crown analysis tend to be at least as accurate, if not

more so as compared to manual methods. An example of the automated tree crown analysis output from their research is presented in figure 1. As is illustrated in this figure, these sorts of algorithms can deduce tree distribution and canopy diameter from a high resolution image. Crown closure and stand area are other variables that can be measured in this manner, as well as tree height, which is sometimes measured using the length of visible shadows.

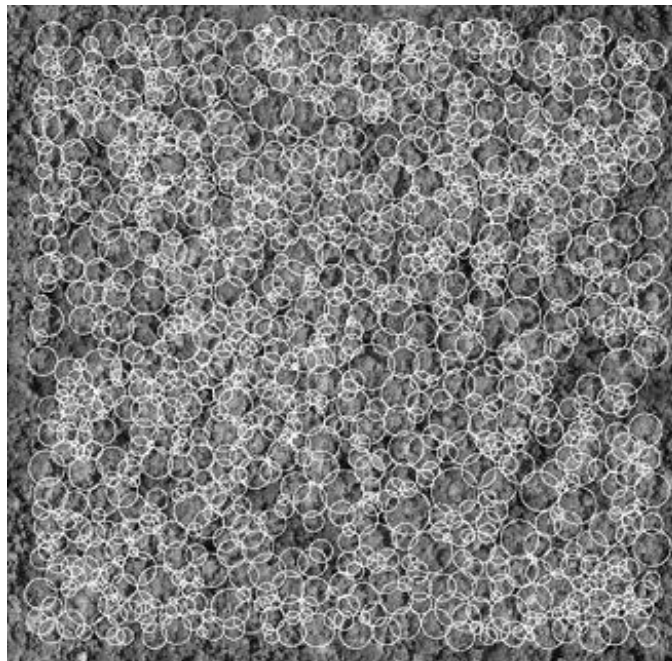


Figure 1: Graphic output from Palace et al.'s (2008) automated tree crown analysis algorithm.

White circles represent the automatically identified tree crowns and their respective circumferences in tropical Amazonian rainforest.

1.5.2 Medium-scale passive remote sensing

Medium-scale passive remote sensing images refer to those with a spatial resolution on the order of about twenty to one hundred meters per pixel captured by sensors aboard such satellites as France's Systeme Pour l'Observation de la Terra (SPOT) or Landsat. At this

resolution, forest structure is exhibited at the subpixel scale which prohibits direct geometric observations of forest structure. As such, various classifying algorithms, statistical methods, and/or correlations with other measurable variables are leveraged as proxies for forest structure. Since structure must be deduced using non-direct methods, medium-scale passive remote sensing techniques tend to be less accurate than fine-scale methods. That being said, medium-scale images tend to be much more accessible, if not free, and allow for consistent temporal observations over time. Unlike fine-scale approaches, this accessibility allows medium-scale images to be acquired and analyzed at regional to global extents.

1.5.3 Coarse-scale passive remote sensing

Coarse spatial resolution based approaches have similar limitations and benefits compared with that of the medium-scale variety, and often employ similar techniques and correlations. While coarser scales necessarily introduce more uncertainty in their indirect measurements of forest structure, they are also increasingly more available both financially (typically free and downloadable online) and temporally. The various sensors that fall within this category include the Moderate-resolution Imaging Spectroradiometer (MODIS) and Multi-angle Imaging Spectroradiometer (MISR) with approximately 300 meter spatial resolution, the Wide Field-of-view Sensor (WiFS) with 180 meter resolution, and the Advanced Very High Resolution Radiometer (AVHRR) with 1.1 kilometer resolution. The eight day (four day in some locations) temporal resolution of MODIS and the thirty plus years of data collection from AVHRR lend coarse-scale approaches to be well suited for observing changes in forests over time (Lu, 2006).

As discussed above, the nature of medium and coarse-scale remote sensing data is such that forest structure is directly identifiable only at the subpixel level. Thus, in order to deduce any reasonable measure of forest structure from these images, one must employ one or more of the following methodologies: correlation with remote sensing indices such as NDVI, LAI or EVI, classifying algorithms and statistical methods, vegetation and biomass models, and/or scaling with finer-resolution data. It should be noted that because these methods do not directly measure forest structure, they all must be calibrated with either in-situ, fine-scale passive, or actively remote sensed data (Shugart, Saatchi, & Hall, 2010).

1.5.4 Active remote sensing

Whereas passive remote sensing approaches simply sense radiation that is being emitted from a foreign body (either from the sun or the Earth), active remote sensing approaches leverage the ability to sense radiation emitted by a controlled source, such as a laser or radio wave sounder. The manner in which active remote sensing payloads sense the Earth is such that the actual structure of forests can be measured. When emitted radiation is directed towards the Earth, it is reflected back to the sensor in different ways and at different points in time, depending on the distance from the sensor and type of medium that is reflecting the signal (a simplified example is illustrated in figure 2). This variation in reflectance can be used to tease out as important structural forest details such as canopy height and density (Lim, Treitz, Wulder, St-Onge, & Flood, 2003).

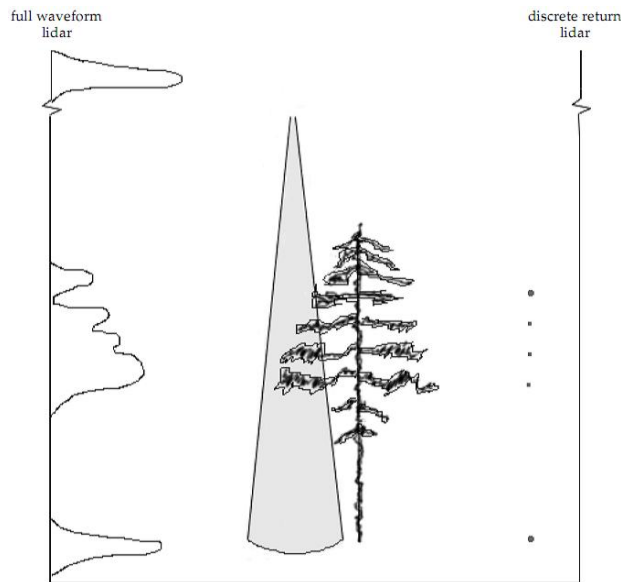


Figure 2: Illustration of how LiDAR response curves would hypothetically behave when encountering above ground biomass, such as a standing tree (Lim, Treitz, Wulder, St-Onge, & Flood, 2003).

Currently, there are two main types of active remote sensing approaches: that which is characterized as using Radio Detection and Ranging (Radar) and that which uses Light Detection and Ranging (LiDAR). These two approaches employ similar methodologies, and often have similar outputs. Various Radar sensors include the Spaceborne Imaging Radar (SIR-C) and numerous different Synthetic Aperture Radars (SARs) aboard various satellites, as well as airborne payloads such as AIRSAR and E-SAR. SIR-C and SAR data provide reliable data over decent temporal scales, but the resolution of these satellite-borne sensors are often similar in resolution to medium-scale passive sensors (at approximately thirty meters). At this resolution it is difficult to directly detect forest structure (Lu, 2006). By weighting the various reflectances and polarities measured in different bands, however, a backscattering coefficient can be calculated, which in turn can be used to deduce forest structure using an empirical relationship

similar to that in figure 3 (Toan, et al., 2004). As with medium to coarse-scale passive remote sensing approaches, a large degree of uncertainty and confounding effects are introduced whenever spatial resolution is larger in scale than the property that is being measured. Airborne Radar sensors do provide the finer-scale resolutions necessary for directly measuring forest characteristics such as canopy height but tend to be too expensive and time-consuming for large scale studies.

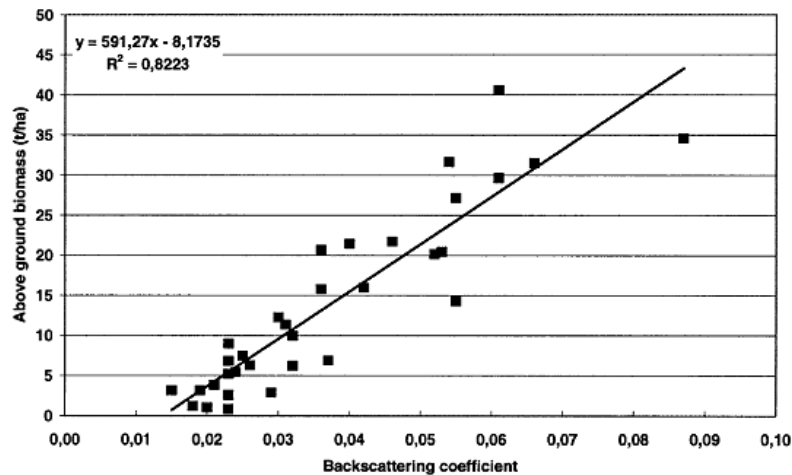


Figure 3: Graphical relationship between backscattering coefficients calculated from SAR instruments and above ground biomass (Toan, et al., 2004).

Similarly to Radar, LiDAR data can come both from spaceborne sensors such as CALIPSO, GLAS, ATLAS as well as airborne instruments such as the Scanning LiDAR Imager of Canopies by Echo Recovery (SLICER) sensor, the Carnegie Airborne Observatory and the Laser Vegetation Imaging Sensor (LVIS). Spaceborne LiDAR data is rarely used for estimations of forest structure, likely because of its coarse resolution. That being said, there is a plethora of researchers currently employing airborne LiDAR data. Just as with airborne passive or Radar

sensors, though, this sort of technique is often cost prohibitive for large scale measurement and monitoring. The methods for measuring forest structure from this data seem to be the most accurate of any remote sensing method, likely because of the combination of high spatial resolution and the ability to monitor vertical structure. An example of an aerially-mounted LiDAR sensor's data in figure 4 exhibits the fine-scale variation in canopy height and density of Amazonian tropical forest (Lefsky, et al., 2002).

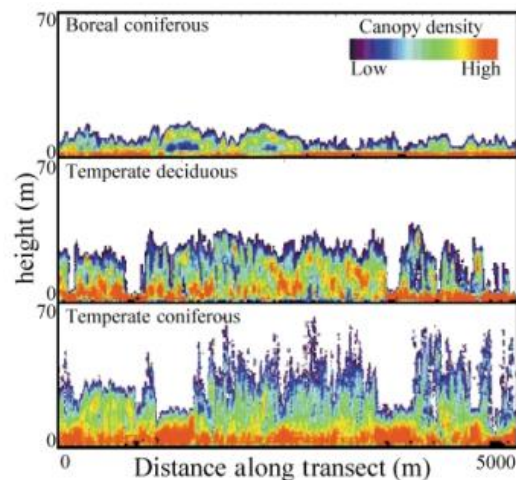


Figure 4: Measurements of forest canopy structure as measured from the SLICER sensor, which exhibit variations in canopy density and canopy height for different types of forests (Lefsky, et al., 2002).

1.6 Dry tropical forests

Dry tropical forests (as compared to wet and moist tropical forests) comprise the biggest proportion of tropical forests and represent an estimated 22% of the Earth's total forests. Given its relative abundance compared with wet tropical forests, the dry tropical forest biome receives much less public, media, and scientific attention (Murphy & Lugo, 1986; Miles, et al., 2006;

U.N.). This type of forest appears to be understudied due to both methodological and economic factors. From a remote sensing point of view, this likely has to do with the complexity inherent in the assessment of dry tropical forests. This includes difficulties measuring multi-story canopies and surface reflectance issues. In addition, existing algorithms are typically designed either for less complex temperate, or more complex moist biomes that saturate when applied to dry tropical rainforests (Fensholt, Rasmussen, Nielsen, & Mbow, 2009). Many dry tropical forests fall within the boundaries of relatively under-resourced and developing countries, complicating data collection. In developing countries, scientific endeavors compete for limited resources and are often relegated on the list of priorities, while a lack of developed infrastructure makes in-situ studies more difficult and costly. This study offers the opportunity to provide data on an under-researched region of dry tropical forests known as the Dry Deciduous Lowland Forests of Mozambique.

1.7 Forest use in the Sofala Province of Mozambique

Section 1.1 outlined the role of forests both as a part of a dynamic global environment and as an agent in anthropogenic social, economic and political systems. The latter role is necessarily true in Mozambique, where forests contribute to many of the good and services utilized by its wider population. Forests permeate the daily lives of many Mozambicans, providing energy (80% of the country's energy demands are met through wood and charcoal combustion), a habitat for food (80% of the country's populated area relies on bushmeat from forests as a source of protein), and even a source of medicine (10% of Mozambique's flora are used in traditional medicine practices) (ARD, Inc., 2002). Additionally, forests are seen as economic drivers by providing natural resources such as lumber and pulp that can be sold in

global markets. The use of forests for subsistence needs such as energy, food and medicine promotes interaction with, and connection to local forests. However, the utilization of forests solely for lumber products often introduces a disconnect between these forests and human consumers. This disconnect can in turn lead to forest management practices that do not ensure the long-term viability of forest ecosystems (Friedmann & McNair, 2008). In fact, 90% of harvested Mozambican lumber is absorbed by the Asian market, adding an even larger gap between consumers and forests (Umuntu Media, 2012). Consequently, many (and increasingly more) Mozambican forestry concessions have multinational owners based in China or Hong Kong (Environmental Investigation Agency, 2013). Although the national or cultural background of a forestry concession's management does not necessarily determine its harvesting practices, foreign owners may focus more on wood as a product and not the forest as a whole. Without a culture-based sensitivity to the forest as a life-sustaining ecosystem, foreign developers are likely to neglect the impact of harvesting on broader ecological processes, in addition to the nutritional and medicinal functions of the forest. With a one-dimensional view of the forest, developers will tend to employ more environmentally and socially extractive methods of harvesting (Fortin, 2013). In the Sofala province where this study is focused, 72% of the companies involved in harvesting timber have not engaged in any forms of reforestation, shedding light on the extractive and unsustainable approaches that dominate lumber harvesting operations in this area (Savcor Indufor Oy, 2005).

2 Project Description

2.1 Research Hypotheses

1. (a) Remote sensing analysis utilizing crown delineation software can effectively identify and measure tree crowns in a manner consistent with in-situ data. (b) This methodology can be consistently employed over the range of forest types (from open woodlands to closed canopy) found within the Dry Deciduous Lowland Forests of Mozambique.
2. Using this analysis, there will be detectable and significant structural dissimilarities in forests that undergo different disturbance regimes.
3. This methodology will be able to link changes in forest structure to various forest management practices.

2.2 Study Area

The study area is located within the Dry Deciduous Lowland Forest region, approximately 30 kilometers south of the Zambezi River within the Cheringoma District, in the Sofala Province of Mozambique (Campbell, 1996; Wild & Barbosa, 1967). Figure 5 displays the study area overlaid on a land cover map and illustrates the three main land classifications present: dense (or closed canopy) forests, open woodlands and prairies. This particular site was chosen for a number of reasons, in part because of the relatively understudied and remote nature of this area. Additionally, research within this study area leverages and strengthens preexisting, longitudinal relationships among researchers at the University of Virginia, the University of Southern Illinois and the University of Eduardo Mondlane in Maputo, Mozambique as well as the operators of the timber concession, TCT Catapu, in Sofala. As one of only two Forest Stewardship Council (FSC) certified operations in Mozambique, and only a handful within the

entire African continent, TCT Catapu offers a uniquely managed, periodically-disturbed forest unlike anywhere else on the continent (FSC Forest Stewardship Council). A site visit in 2009 confirmed the novel and sustainable practices being employed by this operation, including the designation of 16 hectare unmanaged and unharvested “set aside areas” per 1000 hectares and a 32 year, selective logging rotation among blocks within the property. This type of rotation harvesting creates a spectrum of blocks that exhibit varying and predictable amounts of time since the most recent harvesting disturbances. Lastly, the owners of this forestry have been known to welcome scientific teams on their property and can provide the local assistance necessary for conducting field research in such a remote location. For this reason, all in-situ data collection was conducted in cooperation with TCT Catapu within their concession limits.

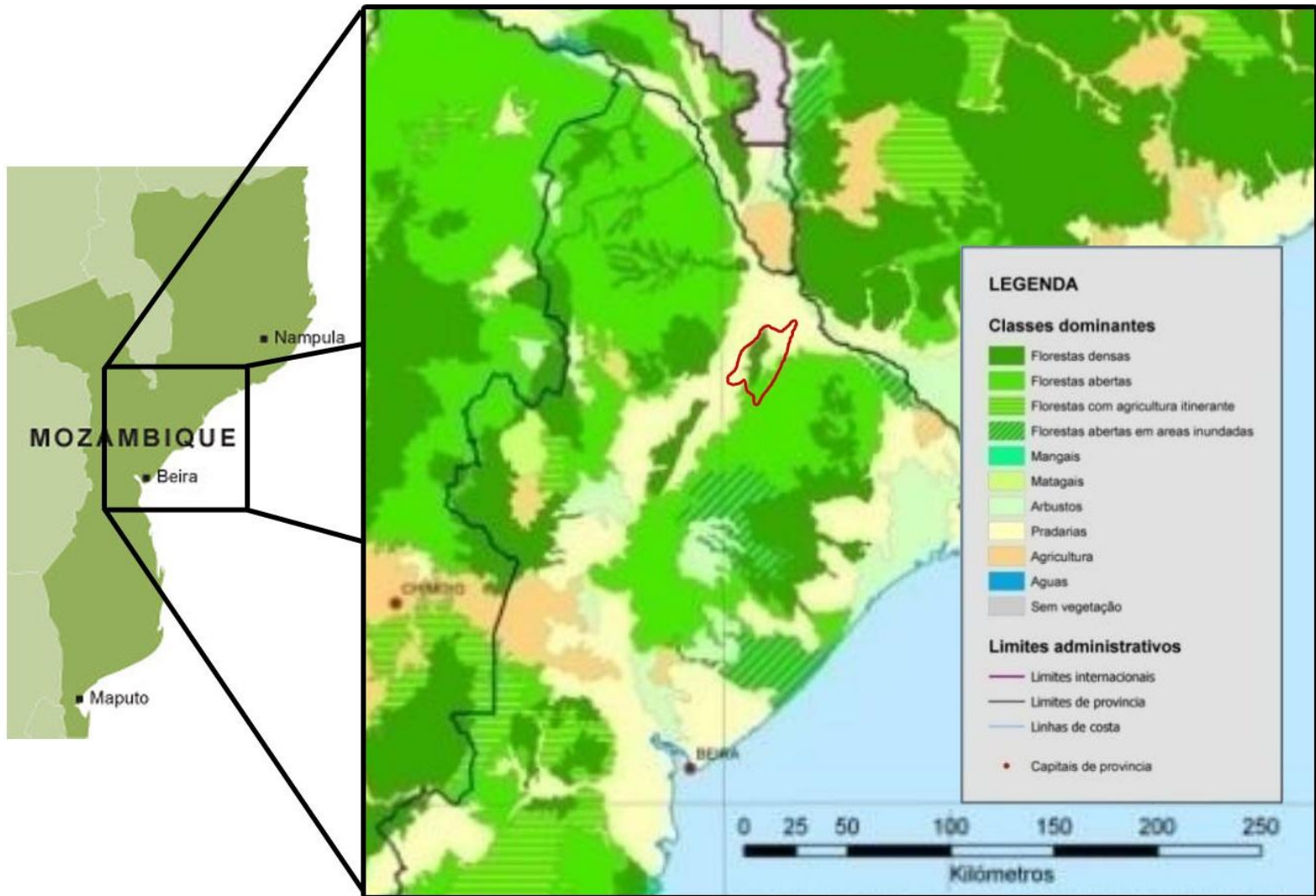


Figure 5: Land cover map of the Sofala province adapted from Macuacua (2012) with the study area outlined in red. The legend lists the various “classes dominantes” (ruling classes) of this area, three of which fall within the study area: “florestas densas” (dense forests), “florestas abertas” (open woodlands) and “pradarias” (prairies).

In addition to the forest concession operated by TCT Catapu, the study area includes the northern adjacent concession managed the Mozambican-Chinese partnership, EDM Limitada. Figure 6 illustrates the study area in more detail and identifies the TCT Catapu (yellow) and

EDM (orange) concessions. While there was no direct communication with EDM's management, it is included as part of the study area because of its shared border with, but distinctly different harvesting methods as compared to TCT Catapu. Whereas TCT Catapu employs the lower impact, FSC certified rotational management strategy described above, EDM's operations bear no such certification. In fact, the entire concession was intensely harvested from 2009 to 2012 and has since been abandoned. During this time period, several main species (including *Millettia stuhlmannii*, *Cordyla africana*, and *Combretum imberbe*) were felled so aggressively, that this area is no longer a viable option for subsequent forestry. It has been roughly estimated that 8,000 to 10,000 m³ of lumber was extracted from the 14,000 hectare concession during those four years. While this area has been noticeably thinned on the ground, it is difficult to distinguish via visual inspection of satellite images. This is a function of the diversity of the region's forests and the many noncommercial tree species that remain standing after harvesting. An additional difference in the harvesting techniques between these two concessions is the degree to which each felled tree is utilized. EDM tends to focus on lumber from minimally flawed logs, often leaving the majority of the felled tree on the forest floor, while securing the prime section of the bole. TCT Catapu, on the other hand, has developed a creative operation that seeks to maximize the use of available lumber through their on-site lumber mill, complemented by wood turning and carving stations. By finding a use for smaller dimensional lumber and creatively utilizing odd-shaped pieces from stumps and branchwood, TCT Catapu is able to realize far more lumber volume per felled tree than more traditional harvesting operations. It should be noted that this information was not gathered empirically, and was instead acquired through personal communication with the TCT Catapu management and lumber suppliers in the Provincial capital of Beira.

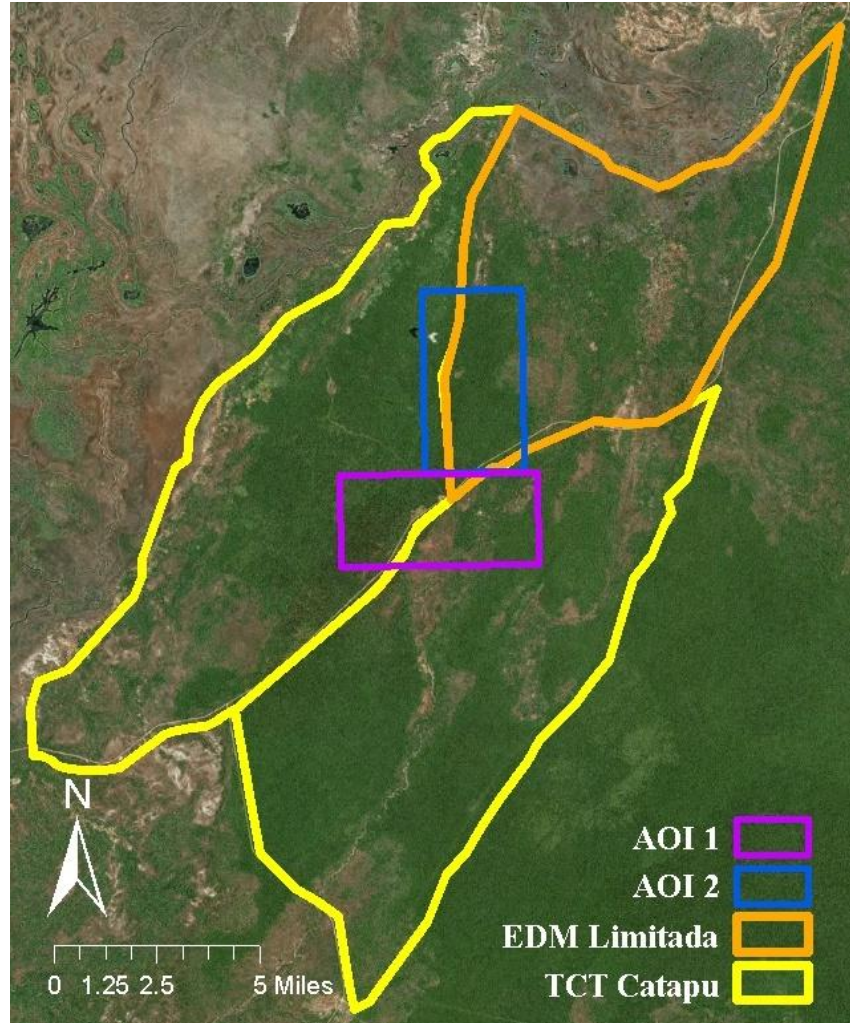


Figure 6: Map of the study area centered on coordinates -18.05, 35.18 that represents the amalgamation of the concessions, TCT Catapu in yellow and EDM Limitada in orange. The more specific areas of interest are additionally outlined.

Within the main site described above, two areas of interest (AOIs) were chosen based on forest disturbance regime, field data locations and remote sensing data availability. For each of these areas of interest, one WorldView2 and one GeoEye1 image (each with panchromatic and multispectral bands) were obtained as outlined in section 3.1. The first area of interest (AOI1 –

purple outline in figure 6) was chosen because it includes contiguous plots where field data was collected, which allows for proper calibration of the crown delineation software with in-situ measurements. Within AOI1 there is range of forest types from open woodlands to closed canopy forests, allowing for comparison of forest properties across these types of forests. Additionally, AOI1 falls within the boundaries of the TCT Catapu concession, where harvesting statistics are known, allowing for the comparison of different harvesting blocks that have undergone varied and known disturbances.

The second area of interest (AOI2 – blue outline in figure 6) falls within both the TCT Catapu and EDM concessions. This allows for a comparison of harvesting approaches in highly similar, adjacent closed canopy forests. This AOI contains mostly closed canopy forests, but includes a small section of woodlands along its central eastern edge. Figure 7 outlines the locations of forest types within each area of interest.

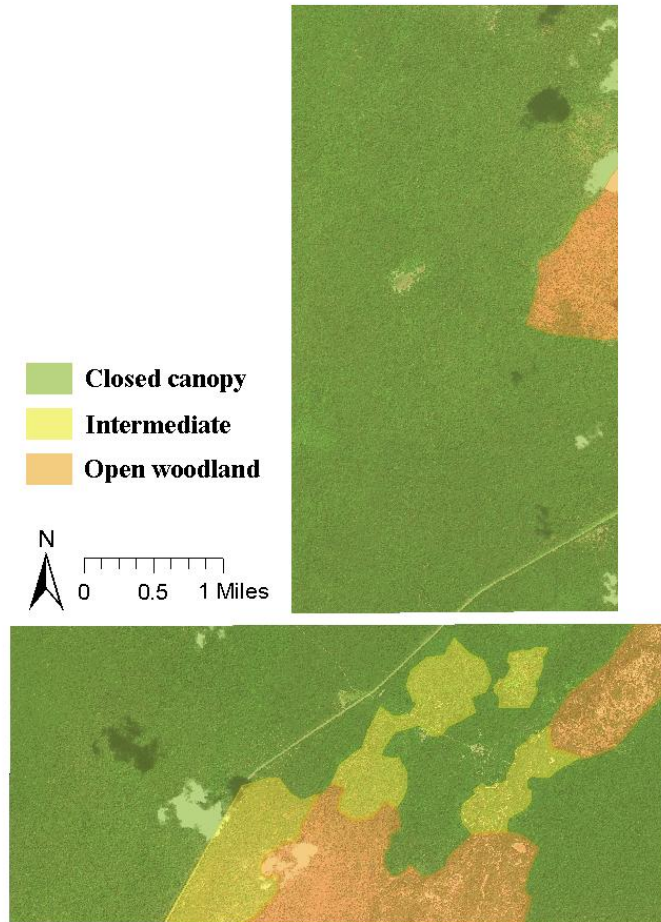


Figure 7: Map of each AOI and its classified forest types overlaid on WorldView2 true color imagery.

3 Methods

To test the aforementioned hypotheses, a number of techniques were employed to measure, gather and analyze an appropriate dataset. A general work flow is presented in the following paragraphs, and illustrated visually in figure 8.

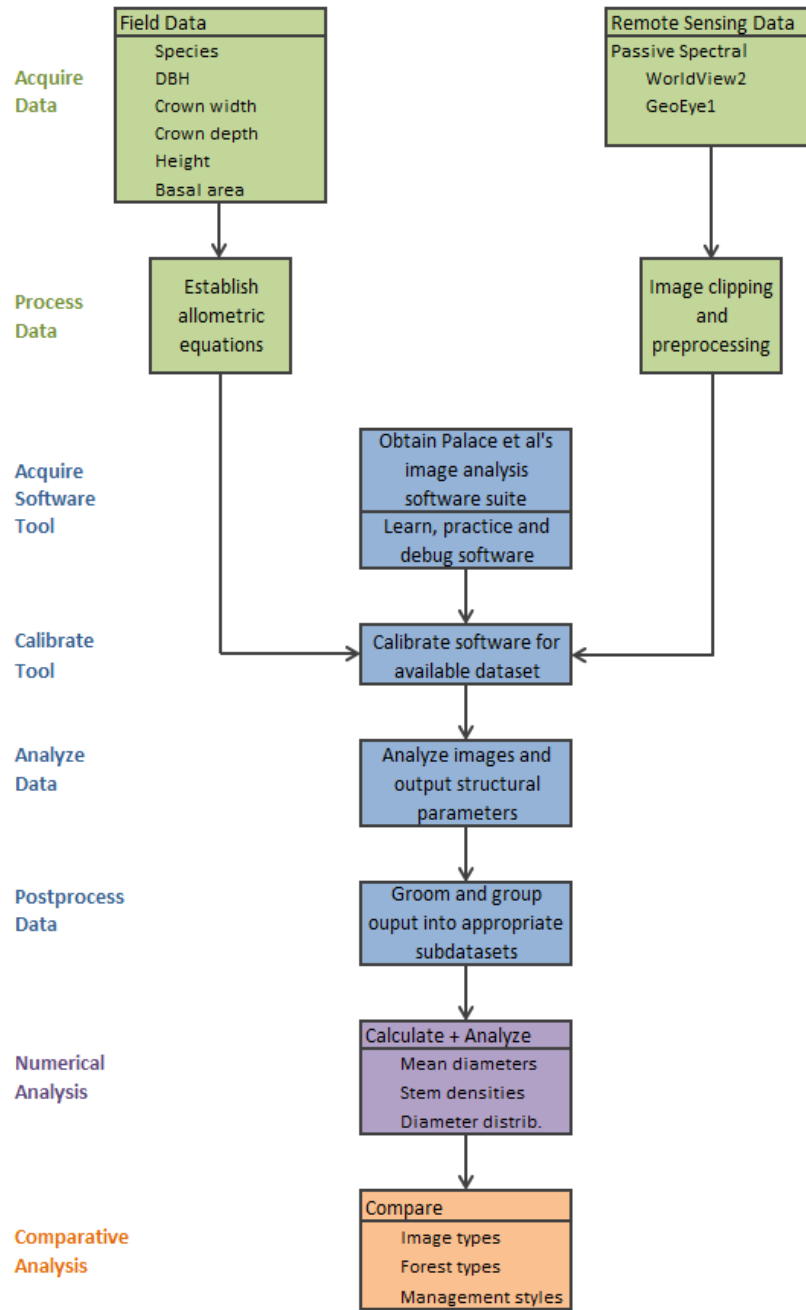


Figure 8: Work flow diagram for this study.

3.1 Field data acquisition

After the specific sites were selected, the data collection phase began. The two main sources of data were categorized as either in-situ field data or remote sensing data. Each of these datasets required a distinct methodology for collection as outlined in the following paragraphs

In-situ data collection is an essential step in this study for two main reasons. First, in-situ data was essential in calibrating the subsequent analytical tools. Secondly, it provided the basis for developing a series of allometric relationships. In order to ensure that the requisite data was properly collected, a hybrid methodology, adapting those described by Asner et al. (2002) and Broadbent et al. (2008) was employed. These studies articulate field sampling methods for collecting the measurements necessary for the calibration of a remote sensing tools similar to those used in this study. A list of in-situ measurements and observations was developed which balanced the temporal and financial costs associated with collecting field data and the need for a robust dataset. Table 1 lists these properties and their associated measurement techniques.

Table 1: In-situ field measurements and techniques.

Tree Property	Measurement Technique
Species	Field guides - local knowledge
Diameter at breast height (DBH)	DBH tape
Crown width	Handheld laser range finder
Crown depth	Laser range finder + clinometer
Tree height	Laser range finder + clinometer
Basal area of nearby trees	Basal area prism
Basal area of taller nearby trees	Basal area prism

Collecting tree species enables quantification of diversity and allows for the application of previously developed species-specific allometric relationships in future studies utilizing this dataset. Each species was identified by name according to the local dialect, Sena. The Sena

names were then converted to their scientific names according to a table presented by Palgrave et al. (2007). Diameter at breast height (DBH) was collected using a DBH-specific measuring tape. This is an important structural property of the tree and is useful in estimating other unmeasured tree properties via preexisting allometric equations, such as above ground biomass.

Tree height, crown width and crown depth are less commonly measured structural properties, but nonetheless play an important role in describing the geometry and other characteristics of the individual tree. In particular, in-situ crown widths were instrumental in developing a baseline dataset for subsequent calibration of the analytical remote sensing tools. These widths were measured along the cardinal N-S and E-W dimension using a laser range finder positioned perpendicularly beneath the outer boundary of the crown and measuring the distance to a surface situated perpendicularly beneath the opposite crown boundary. Tree height and crown depth were measured by standing in a position where the base of the crown, the base of the trunk, and the vertical extent of the tree could viewed simultaneously at approximately ten meters from the tree trunk. A laser range finder was then used to measure the perpendicular distance of the observer from the tree (x) as illustrated in figure 9. A clinometer was used to measure the angles to the base of the trunk (\angle trunk base), the base of the crown (\angle crown base), and the top of the crown (\angle tree top). Using simple trigonometry, these angles and distances were converted to tree height and crown depth. The basal area of trees surrounding each of the measured trees was collected using a basal area prism, while noting which of the surrounding trees were taller than the measured tree. These measurements were crucial in estimating the competitive environment of the tree, potential crown exposure and tree canopy class (such as dominant, codominant, intermediate, or overtopped) (Nylan, 2002).

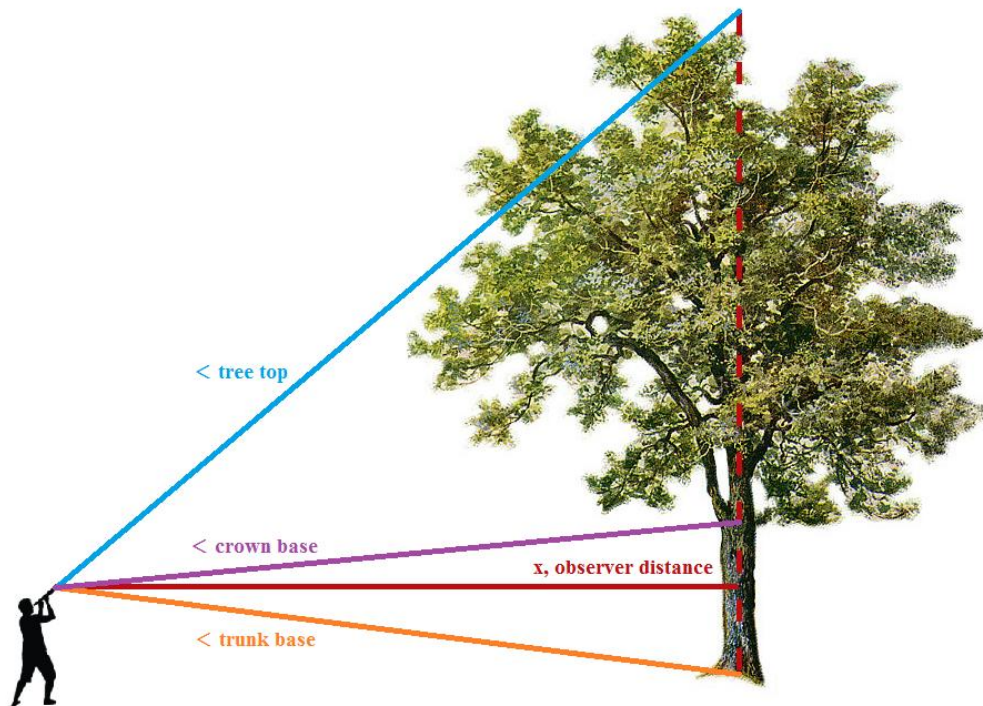


Figure 9: Illustration of the method used to measure tree height and crown depth using a laser range finder and clinometer.

After arriving in country, specific plots were chosen in collaboration with the TCT Catapu forestry management, based on forest type and disturbance characteristics. At least two different plots were chosen within closed canopy and open woodland type forests, with at least one plot for each forest type exhibiting low anthropogenic disturbance and having no recent history (within about forty years) of logging. For practical reasons, the plot selections were all within walking distance (within about an hour) from the main camp. Four randomized line transects of 500 meters were identified within each plot. A stratified sampling technique was employed based on the anticipated DBH distribution. This sampling approach attempted to avoid an overrepresentation of smaller trees and underrepresentation of larger trees by assigning a sampling percentage to each DBH class (Keller, Palace, & Hurtt, 2001). In this manner, the

transect was traversed and a subplot was designated at 25 meter intervals. At each subplot, the four nearest trees exhibiting the minimum DBH requirement of 10 centimeters was selected, their DBH measured and their species noted. Each tree was then assigned a randomly selected one digit number, which determined whether that tree's DBH class necessitated additional measurements (as presented in table 1). The stratification scheme used in the field is presented in table 2.

Table 2: Stratification scheme for determining which trees receive a “full” measurement. If the random number assigned to that tree falls within the range presented in column three, then a “full” measurement was undertaken, including all measurements presented in table 1. Otherwise, only the DBH and species were noted.

DBH class	Sampling percent	Random #'s for full measurement
10 – 20 cm	20%	0 – 1
20 – 30 cm	40%	0 – 3
30 – 40 cm	80%	0 – 7
40 cm +	100%	0 – 9

By following the procedure outlined above a total for 320 sampling locations were identified along 16 transects (displayed in figure 12) and 1280 trees were selected for DBH measurement. Of those 1280 trees, only 960 have their associated species noted. This was due to the lack of field guides available for a number of days during an unforeseen extended national holiday. The DBH bins for all 1280 trees are presented in figure 10, which illustrates an expected decrease in tree frequencies as DBH increases. The numbers of trees in each bin which were fully measured are presented in figure 11, which shows the relatively even distribution of measured trees in each DBH class. In all, a total of 469 trees were fully measured as described in

table 1, which represents a 50% larger dataset than the suggested sample population of 300 trees required for calibration as presented by Asner et al. (2002).

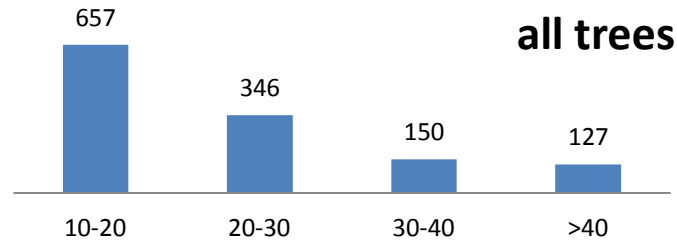


Figure 10: The number of trees which fell into each DBH bin class, where DBH was measured in centimeters.

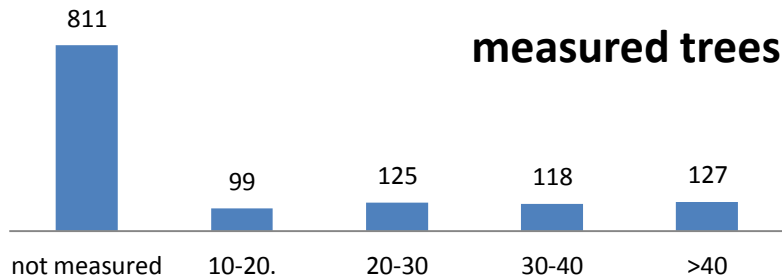


Figure 11: The number of trees that were fully measured as described in table 1 within each DBH class, where DBH was measure in centimeters.

Additional data, in the form of historical records was also collected with the help of the TCT Catapu management. The locations and statistics associated with each harvesting block were shared in order to provide insight into the anthropogenic disturbances experienced by different areas within the concession. Figure 12 presents the locations of the various blocks that fall within AOIs 1 and 2, while table 3 summarizes the available harvesting data for each of these

blocks. Additionally, the TCT Catapu management provided anecdotal information related to the state of lumber harvesting in the Sofala province of Mozambique. This included generalized information about areas that experience high or low harvesting disturbances and methods of harvesting present in the region.

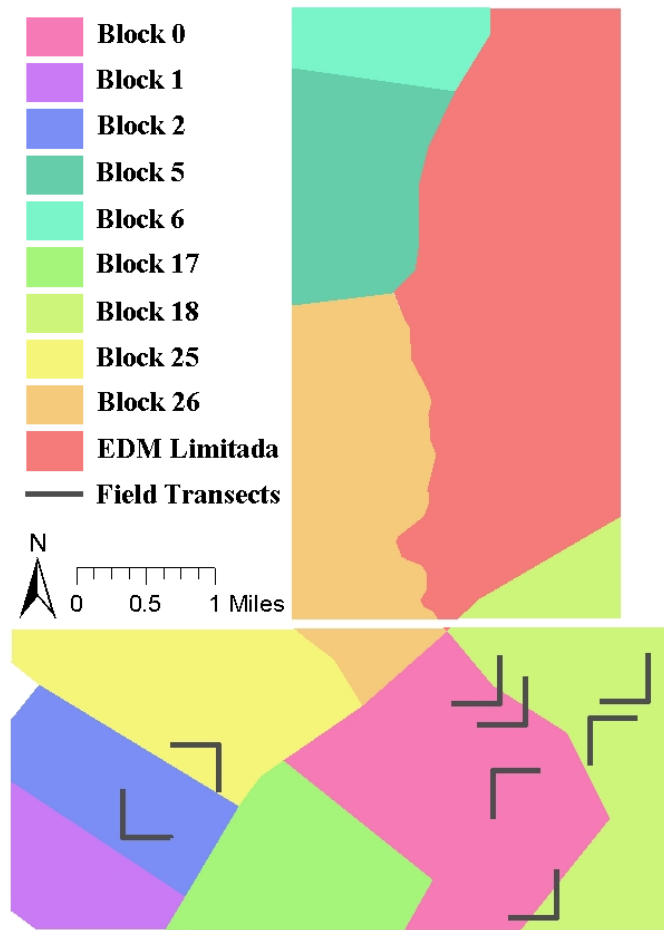


Figure 12: Representation of the various TCT Catapu harvesting blocks within each area of interest, as well as the area managed by EDM Limitada and the field transects traversed for this study.

Table 3: Summarized harvesting data for the blocks that fall within AOIs 1 and 2, including: total area, the main years of harvesting (several blocks experience additional, yet significantly smaller periods of harvesting), and the total volume of lumber harvested (for the three main species – Panga Panga, Chanfuta, and Mutondo).

Block	Total area (ha)	Harvest year	Volume harvested (m ³)
1	385	1996	1,318
2	339	1997 – ‘98	783
5	1903	2003	3,170
6	1540	2001	1,465
17	1960	2006 – ‘07	2,301
18	5352	n/a	0
25	1093	2004 – ‘05	2,543
26	1585	2005 – ‘06	2,536
0	1039	n/a	0

3.2 Remote sensing data acquisition

An appropriate remote sensing dataset (or “image”) is a necessary complement to the in-situ data collected on the ground. As discussed previously, there are several categories of remote sensing data. In order to choose the most appropriate dataset for the purposes of this research, several factors were taken into account, including spectral range, spatial resolution, availability and cost. The most limiting factor was spatial resolution. Since this study is focused on structural properties at the individual tree level, remote sensing datasets with spatial resolutions larger than an average tree’s canopy are immediately excluded. The next factor to consider is the spectral range associated with each remote sensing dataset. This is a less exclusive data requirement, as the analysis software is compatible with a range of spectral inputs, including panchromatic and hyperspectral as well as those derived from light detection and ranging (LIDAR) techniques. Cost and availability are obvious limitations associated with any type of data collection and ended up being a significant driver in data acquisition process.

Active LIDAR-based datasets are promising for this type of research because they represent measurements taken in three-dimensional space. This dataset allows for the analysis of both horizontal and vertical tree characteristics, whereas passive remote sensing techniques are confined to the two-dimensional, horizontal plane. Airborne-based LIDAR datasets provide the benefits of this three dimensional dataset with fine scale spatial resolution, but at costs and within a restricted sampling area that were prohibitive for this study. Satellite-based LIDAR datasets such as those collected aboard the Geoscience Laser Altimeter System (GLAS) or the Ice, Cloud and land Elevation Satellite (ICESat) exhibit resolutions that are too coarse, and would require calibration with alternative, higher resolution sources (Choi, et al., 2013; Defibaugh y Chavez & Tullis, 2012).

LIDAR-based datasets are not necessary, as this study is well suited to use two dimensional image analysis instead. These passive remotely sensed datasets have been proven to be adequate inputs in previous tree structure analyses as long as they exhibit sufficient spatial resolution (Broadbent, Asner, Pena-Claros, Palace, & Soriano, 2008; Asner et al., 2002; Palace, Keller, Asner, Hagen, & Braswell, 2008; Chambers, et al., 2007; Culvenor, 2002). As such, several passive, fine-scale remote sensing datasets were explored. These are presented in table 4 with their respective spectral packages and spatial resolutions.

Table 4: Potential sources of high resolution passive remote sensing data, their respective spectral packages and spatial resolution for each band at nadir.

Satellite payload	Spectral package (spatial resolution)
WorldView2	Panchromatic (0.46m) + 8 multispectral bands (1.85m)
WorldView1	Panchromatic only (0.5m)
QuickBird	Panchromatic (.65m) + 4 multispectral bands (2.62m)
GeoEye1	Panchromatic (.41m) + 4 multispectral bands (1.65m)
Ikonos	Panchromatic (.82m) + 4 multispectral bands (3.2m)

The archives of the five satellite datasets listed in table 4 were explored for this study's areas of interest with the help of a third party proprietor. Unfortunately, these datasets are limited by the remote location of these areas of interest, and by relatively brief archive histories (many of these satellites have only been deployed in the last decade). The entirety of the data available for purchase for this study's areas of interest for each of the five satellite payloads is presented in table 5. As can be seen, only thirteen images were available in total, even after relaxing image restrictions such as maximum cloud cover and maximum angle off of nadir. Of these images, only five were "clear" (less than 10% cloud cover) and only seven include both areas of interest. Three images (highlighted in green in table 5) were captured in clear conditions and are of sufficient geographical extent to include both areas of interest. Of these, only the WorldView2 and GeoEye1 images provide multispectral datasets (crucial in masking clouds, roads and ground during analysis). Thus, the two images that meet the quality standards necessary for this study were selected. One WorldView2 image taken on December 16, 2012 and one GeoEye1 image taken on June 8, 2010, were identified and purchased for subsequent analysis. Fortunately, the WorldView2 image was taken within six months of field data collection (during June, 2012) and exhibits the relatively limited degree of change ideal for proper calibration. It should be noted that the measurements taken in the field between the colder, dry season (June) and the hotter, wet season (December) are relatively stable since there is minimal change in forest structure during this period. The GeoEye1 image was taken over two years prior to the WorldView2 image and thus allows for a temporal comparison.

Table 5: Available datasets for this study’s areas of interest (AOI1 and AOI2) and their associated payload and capture date. Red highlighting denotes less than ideal conditions, including high cloud percentage, noticeable attenuation (“hazy”) and limited spatial expanse.

Satellite payload	Date	Extent available	Notes
WorldView2	1/28/2012	AOI2	Cloudy
	4/16/2012	AOI2	Cloudy
	12/16/2012	AOI1, AOI2	Clear
WorldView1	3/27/2013	AOI1, AOI2	Cloudy
	2/22/2008	AOI2	Cloudy
	3/19/2008	AOI2	Cloudy
	1/6/2011	AOI1, AOI2	Cloudy
	1/14/2011	AOI2	Cloudy
	5/30/2011	AOI2	Clear
	6/16/2011	AOI1, AOI2	Clear
	QuickBird	n/a	n/a
GeoEye1	6/8/2010	AOI1, AOI2	Clear
	9/15/2010	AOI2	Clear
Ikonos	8/28/2012	AOI1, AOI2	Hazy

3.3 Field data processing

Upon selection of the requisite datasets, a series of preprocessing steps are necessary before analysis begins in earnest. First, the species associated with each sample was translated from Sena to its scientific name via a table developed by Palgrave et al. (2007). The in-situ data was then aggregated and transcribed into Microsoft Excel. After the data was inputted and checked for consistency, derivative measurements were calculated and relationships among tree geometry were explored. Figures 13 and 14 display the relationship between DBH and average crown width for the full population of measured trees on linear and logarithmic scales, respectively. Figure 15 displays the disaggregated contributions from the woodland and closed canopy samples for the same data. Figure 16 shows a similar disaggregation, but based instead on the surrounding basal area collected for each tree sample. In this case, dominant trees are defined as those that are taller than 90% of the surrounding trees, codominant trees as those taller

than between 50% and 90% and overtopped trees as those that are shorter than at least half of the surrounding trees. These graphs illustrate the relationship between four sets of variables, including: DBH vs. tree height, DBH vs. crown depth, tree height vs. average crown width, and tree height vs. crown depth. A sampling of correlations among selected in-situ data is presented in Appendix A. This is not an exhaustive representation of the various allometric or other relationships that could be determined, but rather a subset of relevant measures.

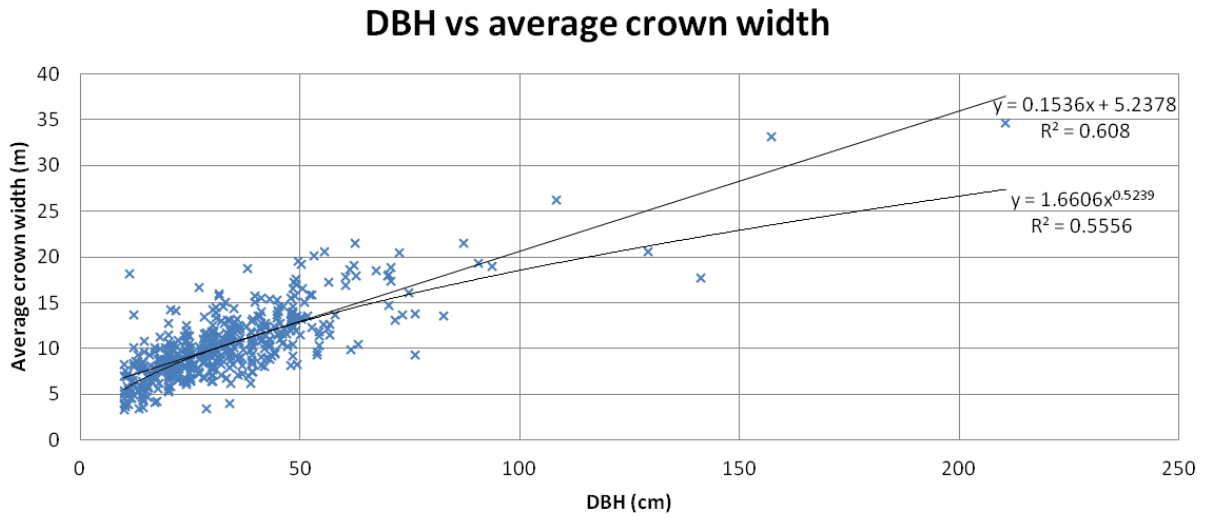


Figure 13: Relationship between DBH and average crown width according to linear axes, and its associated linear and power-based regressions.

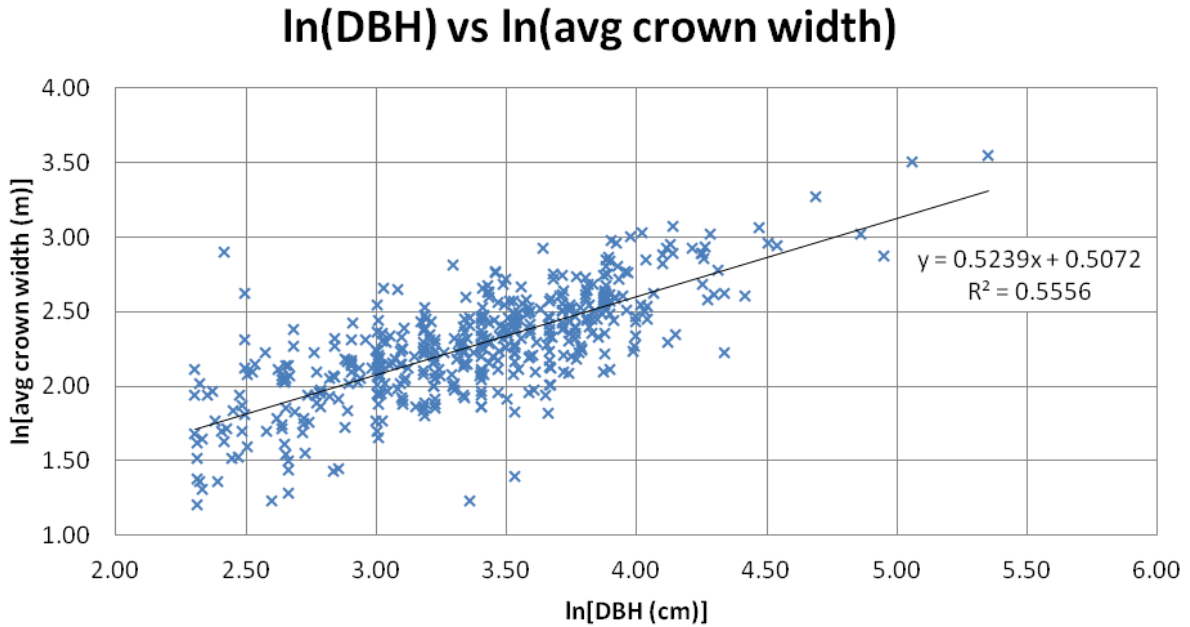


Figure 14: Relationship between the natural logarithms of DBH and average crown widths and its associated power-based regression.

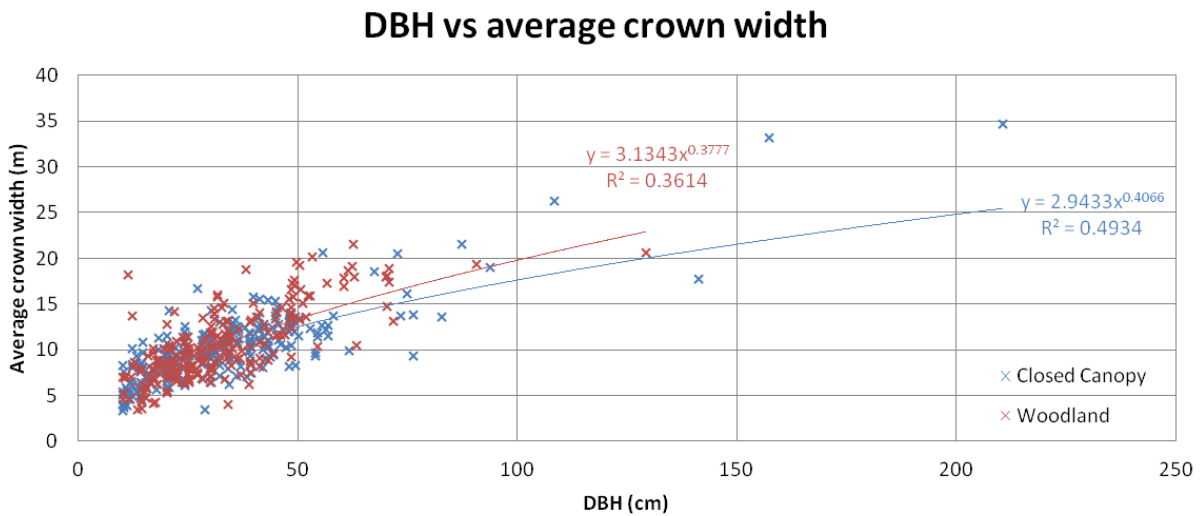


Figure 15: The relationship between DBH and average crown width for the trees measured in closed canopy (blue) and woodland (red) sites and their associated power-based regressions.

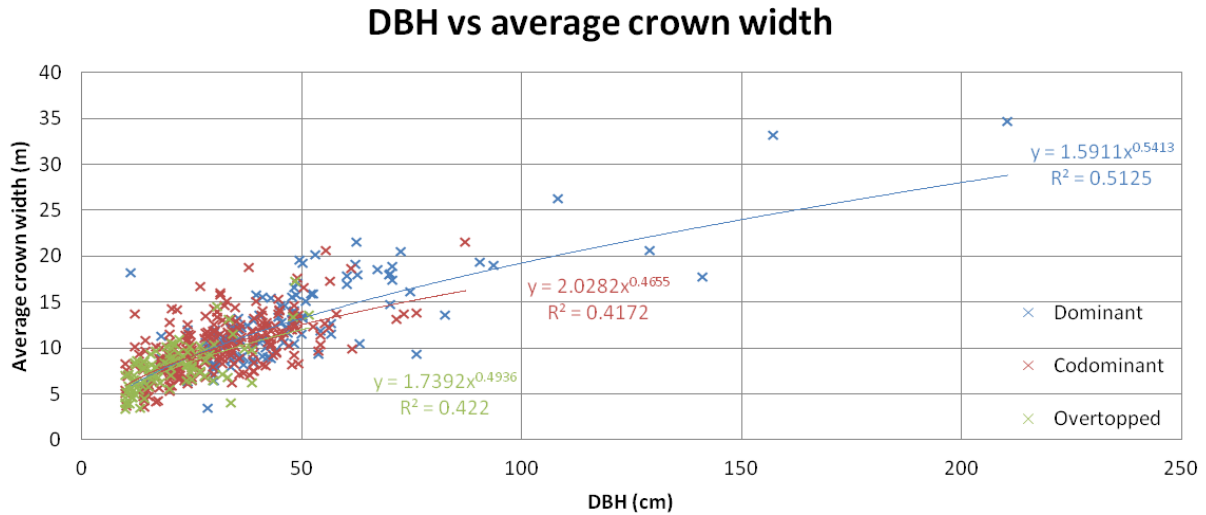


Figure 16: The relationship between DBH and average crown width for the trees categorized as dominant (blue), codominant (red) and overtopped (green) and their associated power-based regressions.

3.4 Remote sensing data preprocessing

Many remote sensing analyses benefit from data preprocessing prior to more in-depth analysis. Methods of preprocessing can vary, but tend to focus on creating a more consistent dataset. This can include removing flagged or inappropriate pixels, such as those providing inaccurate information due to the effects of factors such as clouds or sunglint. Preprocessing may also entail normalizing and combining data across different sources and performing remote sensing corrections. The analytical software that this study employs includes a preprocessing package that enhances consistency and efficiency in the subsequent tree crown analysis.

aims to ensure consistency and efficiency in their subsequent tree crown analysis. Prior to this study, two dataset-specific preprocessing programs had been developed, one for QuickBird and the other for Ikonos images.

Since the remote sensing images in this study came from different sources, the existing preprocessing programs were redesigned to facilitate analysis. Due to commonalities in parent company, certain similarities existed between DigitalGlobe's QuickBird and WorldView2 satellites, as well as GeoEye's Ikonos and GeoEye1 satellites. As such, the existing QuickBird-specific program was used to guide the development of a WorldView2 preprocessing program while the Ikonos program aided in the preprocessing of GeoEye1.

Each of these programs proceeded according to a common protocol, performing the following main operations. The first step included the import and consolidation of a high resolution (about 0.5 to 1 meter resolution) panchromatic image, a slightly coarser (approximately 2 to 4 meter resolution) multispectral image and the geospatial metadata associated with each image. Because WorldView2 and QuickBird datasets incorporate multispectral bands in different orders, an adjustment was made in the importation of bands so that the blue, green, red and near-infrared bands were all correctly assigned. In order to provide appropriately-sized datasets for the tree crown analysis, these programs then partitioned the larger images into multiple smaller "chips." AOI1 and AOI2 were each broken into 98 different 25 hectare chips from their larger 25 km² images.

Several remote sensing corrections were also included in these programs, such as a top of atmosphere and a solar gain correction. These corrections utilize various factors such as solar zenith angle, satellite off-nadir angle and satellite-specific coefficients to create a more consistent dataset across different images and payloads. Although the existing Ikonos and QuickBird preprocessing programs included these corrections, adequate corrections for WorldView2 and GeoEye1 were unable to be developed for this study. Thus, this part of the program was removed and the preprocessing continued without these slight alterations. The next

step applied a moving window filter to smooth images that contain a high level of radiometric variability. Additionally, the coarser, multispectral bands were broken into smaller pixel sizes that corresponded with the higher resolution panchromatic band. The maximum, minimum and mean pixel brightness values were determined to allow for dataset normalization during the tree crown analysis. After these steps were completed, the panchromatic, blue, green, red and near-infrared bands were packaged into geotiffs with their metadata and exported into their respective chips.

3.5 Remote sensing analysis

Following preprocessing, an automated tree crown analysis software suite developed by Palace et al. (2008) was utilized for further analysis. This software suite uses a pattern recognition algorithm to systematically scan remotely sensed images and automatically delineate tree crowns. There are many methods that have been proven successful in delineating tree crowns, including local minima value finding, local maxima filtering, template matching, valley finding, three dimensional modeling and wavelet analysis (Brandtberg & Walter, 1998; Chubey, Franklin, & Wulder, 2006; Popescu, Wynne, & Nelson, 2003; Leckie, et al., 2005; Wulder, Niemann, & Goodenough, 2000; Shugart, Bourgeau-Chavez, & Kasischke, 2000; Pouliot, King, Bell, & Pitt, 2002). The software developed by Palace et al. (2008) leverages a combination of local minima finding and local maximum filtering. This software-based approach was chosen for this study because of its successful use in randomly distributed, high density tropical forests. This stands in contrast to other methods which have focused on less dense, low diversity forests with more regular canopy geometries (Palace, Keller, Asner, Hagen, & Braswell, 2008).

This proprietary software was shared by its authors through a remote connection to two Ubuntu machines at the University of New Hampshire. A remote method was chosen over the use of a local machine, due to the software's complexity and unproven compatibility with foreign computers. As with the preprocessing code developed by the same authors, this program was mostly coded in Python, with the occasional integration of Weave. In its entirety, the suite contains a number of useful remote sensing analyses in addition to tree crown delineation. These include estimates of lacunarity, entropy, angular second momentum, semi-variance and a power spectrum analysis, all of which can provide insight into forest structure (Palace, Keller, Asner, Hagen, & Braswell, 2008). In order to manage the scope of this project, however, it was decided to focus on the analysis provided by the tree crown delineation algorithm.

The program proceeds by importing an appropriately preprocessed remote sensing image, then scanning and identifying local maximum values (according to the "brightness" of each pixel's digital number). It should be noted that the inclusion of a multispectral remote sensing dataset allows for the masking of bright non-canopy pixels through the use of an NDVI filter. From these maximum value locations, an ordinal transect analysis is conducted via linear transects in 360 directions. These transects extend until either an observed drop in brightness from the center maxima or until a rise in brightness between two adjacent pixels reaches a predetermined threshold. At that point, the ordinal transect is ended. The local maximum point approximates the center of the canopy which allows the ordinal transects to extend radially and terminate at the edge of the tree crown. These transects are then integrated and approximated as circles centered at the local maximum to delineate each individual crown. The circle's radius is calculated as half the sum of the longest pair of opposing transects. This circle and its pixels are then removed from the image as analysis continues, iteratively seeking lower local maximum values as

additional “trees” are removed. After this point, the analysis is complete and the software outputs data on the geometry of the delineated crowns.

3.5.1 Software calibration

The software suite can leverage a variety of different remote sensing images to analyze a range of different landscapes. The nuances associated with each of these datasets and geographic sites, however, necessitates that the software be recalibrated whenever a new type of image or forest is introduced into the analysis. Although a variety of terrestrial surfaces have been tested with this software, from Amazonian tropical forests to the Sierra Nevada Mountains in California, this study introduces the untested Dry Deciduous Lowland Forests of Mozambique. Due to this new location, in addition to the utilization of unproven datasets (WorldView2 and GeoEye1 images), a number of calibration steps were undertaken to create the most precise and accurate analysis possible. Throughout the calibration process, the available field data was instrumental in providing a baseline for verification. Visual inspections were also key in comparing iterative adjustments in order to identify the most ideal calibration settings.

The following calibration procedure was carried out for each image type. Separate calibrations were not necessary for each AOI, as the WorldView2 and GeoEye1 images contained both AOIs in one contiguous image swath. Calibration began with the WorldView2 AOI1 image which contained the field measurement transects and had been captured within 6 months of field data collection. The GeoEye1 image was taken approximately 2 years earlier.

As part of the calibration process, the existing code was slightly modified during the debugging and troubleshooting process. Most of these changes were semantic in nature and did not alter the overall function of the program. Two functional changes were necessary, however:

the first relating to a software coding problem and the second incorporating a global normalization scheme. Because of a coding incompatibility in the creation a supplementary “masking” image the section of code associated with this function was removed. Fortunately, the impact on the analysis was minimal since this nonessential process only served as a visual check on the masking process, which was able to be independently verified through other methods.

The second and more significant change was the introduction of a global normalization scheme. Without global normalization, each preprocessed chip was independently normalized based on its maximum and minimum pixel value. As such, chips with anomalously bright or dark pixel values would be represented on entirely different scales than adjacent chips without such extreme values. This would result in specious variation in the tree crown delineation, based on these relatively different scales. Figure 17 illustrates the inconsistency introduced by this type of local normalization at the intersection of four adjacent chips. The top, left chip displays inconsistently large representative tree circles caused by an anomalously bright pixel associated with a tin roof elsewhere in the image. In order to remedy this situation, each chip (inclusive of both AOIs) was consistently normalized based on the global maximum and minimum brightness values determined during the preprocessing step (as outlined in section 3.4). The GeoEye1 images were normalized independently of WorldView2 images.

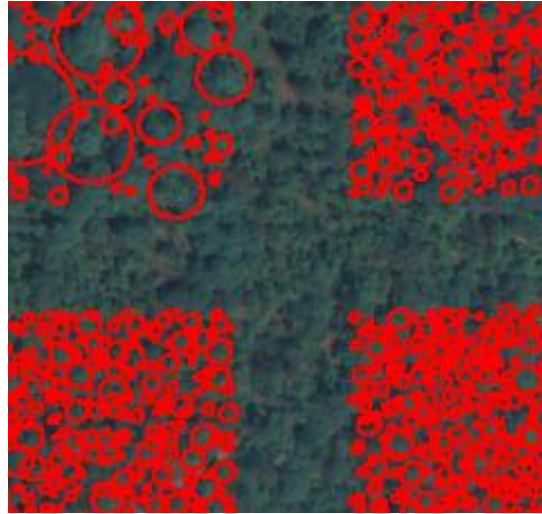


Figure 17: Illustration of delineation inconsistency due to local normalization at the intersection of four chips overlain on a WorldView2 true color image that has been sharpened using the higher resolution panchromatic image (pan-sharpened).

Calibration began by first adjusting the manner in which the program applied an NDVI mask. By applying an upper and lower NDVI threshold, values outside of the specified range were excluded from analysis. This allowed bare soil, clouds, grasslands, water, and most human-made features to be automatically removed from analysis based on their low NDVI values (as compared to forested vegetation). This calibration was undertaken by iteratively adjusting each threshold and inspecting the results for an area that experiences a wide range of NDVI values. After each iteration, the NDVI values of the trees with the brightest 200 pixel values (the first 200 trees to be delineated) were calculated. These values were then associated with the centroid of that tree's location on an appropriate map. Figure 18 displays the delineated tree centroids from several such iterations on a map of the analyzed area. It can be seen upon visual inspection that as the lower NDVI threshold is raised from 0.1 upward, more bare ground is masked out of the image, removing pixels which would otherwise be mistaken as trees from the analysis. As the

lower threshold progressively increases, some vegetated areas begin to be removed the analysis. Through the process of iterative analysis and visual inspection, thresholds were set that removed as much unforested areas as possible without encroaching into the tree canopy. The lower NDVI threshold for both the WorldView2 and GeoEye1 images was set at 0.6, while the upper threshold was set at 0.99.

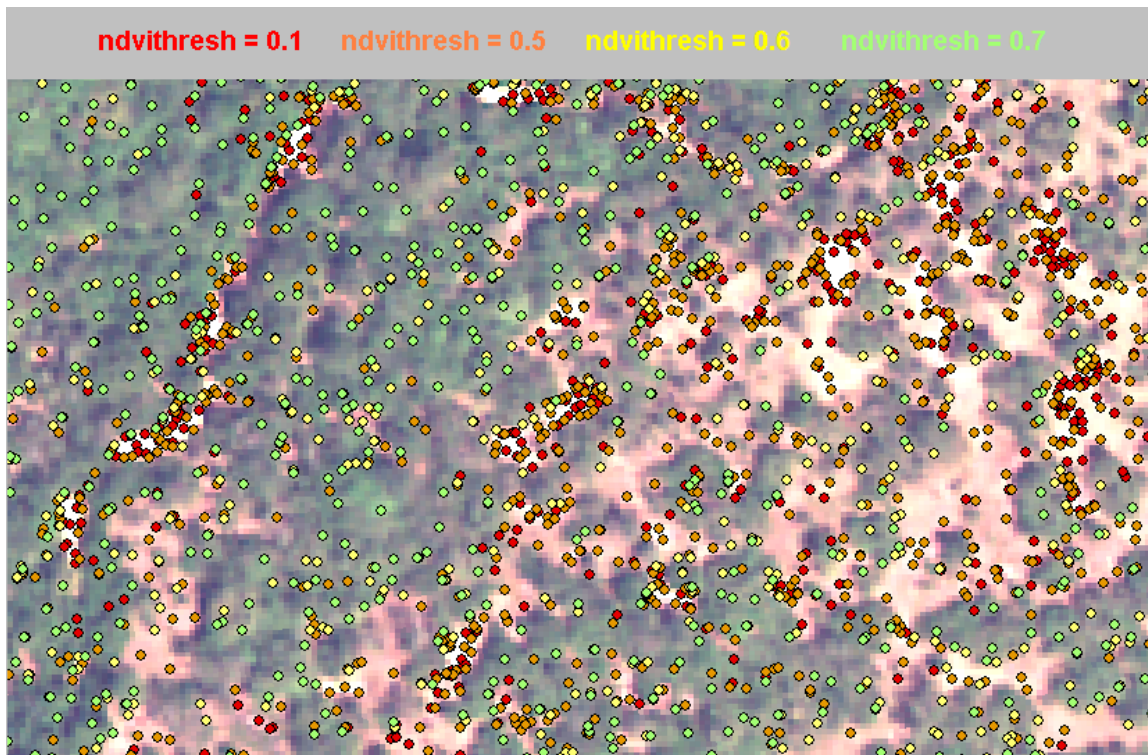


Figure 18: Illustration of delineated tree centroids based on the lower NDVI threshold overlain on the true-color representation of the WorldView2 image within an area of AOI1. The layers of this map are in such an order that the centroid with the largest NDVI threshold value will be visible at any given point. As such, many of the green, $\text{ndvithresh} = 0.7$ locations also represent the locations of $\text{ndvithresh} = 0.6$, 0.5 and 0.1 as well.

With the NDVI thresholds appropriately set, the unmasked, remaining pixels should optimally represent only those areas that exhibit tree canopy cover. Working under this assumption, the main calibration step could begin. This includes the adjustment of two variables, the rise and drop values, which are crucial in properly delineating tree crowns. These two values represent thresholds which, when properly set, terminate the transect during the ordinal transect analysis. As mentioned previously, the aim of this part of the analysis is to end each transect at the edge of the tree crown. The rise value represents an increase in brightness between two adjacent pixels that suggests the edge of the crown has been reached and the transect should be terminated. In contrast, the drop value represents the maximum allowable brightness drop between the peak center brightness and any pixel in the ordinal transect. Adjusting these two values affect both the number and size of the trees that are delineated, and are thus the most important variables in the calibration process.

Due to the complementary nature of the rise and drop values, and their similar impact on analysis, calibrating each of them in turn is not an effective method. As such, they were calibrated “simultaneously” by running the crown delineation algorithm in a sensitivity mode. Essentially, this required placing the algorithm within nested for loops which iterated through a series of assigned values for each variable. The output from each pair of values was imported into Microsoft Excel, Matlab and ArcMap for numerical and visual verification. This iterative, brute force method allowed for a systematic exclusion of certain rise and drop values, until an ideal pair of values was reached.

Numerical and visual comparisons were utilized in order to complement the distinct strengths and weaknesses associated with quantitative and qualitative calibrations. Numerical methods were used to compare outputted data with in-situ measurements of tree crowns. As

elucidated by Asner et al. (2002), it is not realistic to utilize individual tree measurements for calibration due to limitations in geolocation and to temporal changes between in-situ and remote sensing measurements. Additionally, the use of a stratified sampling technique and a minimum DBH threshold contribute to an in-situ dataset that is skewed to include more measurements of larger trees and is therefore not representative of the full population. In-situ data, however, is still important in providing insight into the range of tree crown widths that could be expected from the crown delineation output. Because of these limitations, the in-situ data set was utilized to compare geographically similar transects as opposed to individual trees. In this manner, a 25 meter buffer was added to the sides of each transect traversed in the field. The delineated trees with centroids located within this 50 meter swath were compared to the in-situ dataset for same transect. One closed canopy and one open woodland site (each with four transects) were chosen for calibration comparison, with the others were reserved for subsequent validation. These swaths, in addition to larger 25 hectare chips were also analyzed visually to ensure that the circular tree approximations were located, centered and sized reasonably.

An initially large range of values from 10^{-5} to 10^1 were assigned to each the rise and drop values to ensure a that the range was sufficiently broad. This was then narrowed to a range of 10^{-3} to 10^1 for each variable by removing values that exhibited a consistent maximum diameter (regardless of changes in the complementary variable) that was five times smaller (6.92 m) than the overall maximum diameter (34.61 m) measured in the field. It was also discovered that drop values greater than 10^0 and rise values greater than 10^{-1} saturated such that changes above these thresholds resulted in identical outputs. Visual inspection confirmed that drop values outside of 10^{-3} to 10^0 and rise values outside of 10^{-3} to 10^{-1} led to inaccurate estimations of tree crowns. This was the case for both the WorldView2 and GeoEye1 calibrations. The range of reasonable

rise and drop values was further refined by iteratively removing values that led to exceedingly large or small maximum radii and/or displayed inconsistent delineation upon visual inspection. This led to further narrowing of the range of appropriate rise and drop values for each image as displayed in table 6.

Table 6: Final rise and drop values, in addition to the range of rise and drop values that contributed to reasonable estimations of individual tree crowns after numerical and visual inspection.

	WorldView2 images	GeoEye1 images
Rise value range	0.0075 – 0.0110	0.010 – 0.040
Final rise value	0.0095	0.020
Drop value range	0.060 – 0.100	0.060 – 0.090
Final drop value	0.075	0.070

After the appropriate range of values was defined, a more refined method of comparison was used to arrive at final calibration values. In the manner described above, in-situ measurements from select transects were compared to software-based approximations for trees that fell within the buffered area around each of these transects. The eight transects associated with open woodland site 1 and closed canopy site 2 were randomly selected for this verification step. Since only about thirty trees per transect received canopy width measurements, a couple proxies were used to estimate the canopy diameters for the entire 80 trees identified per transect. Both allometric equations presented in figure 13 were used to estimate canopy width based on each tree's DBH value. This allowed for a comparison of a larger dataset that was not as skewed because the DBH's were measured prior to stratification. That being said, the 10 cm minimum DBH threshold would still contribute to a dataset that excludes the smaller trees present in the software-based approach. As such, a subset of software-derived measurements that were larger

than a certain threshold was included for a more appropriate comparison. This threshold was chosen to be four meters because each of the sites mentioned above had only one tree that measured less than four meters in average diameter. Table 7 displays the average and maximum diameters associated with each measurement or approximation method listed above. All of these values were checked in conjunction with a visual scrutiny of the area in order to select the most appropriate calibration settings.

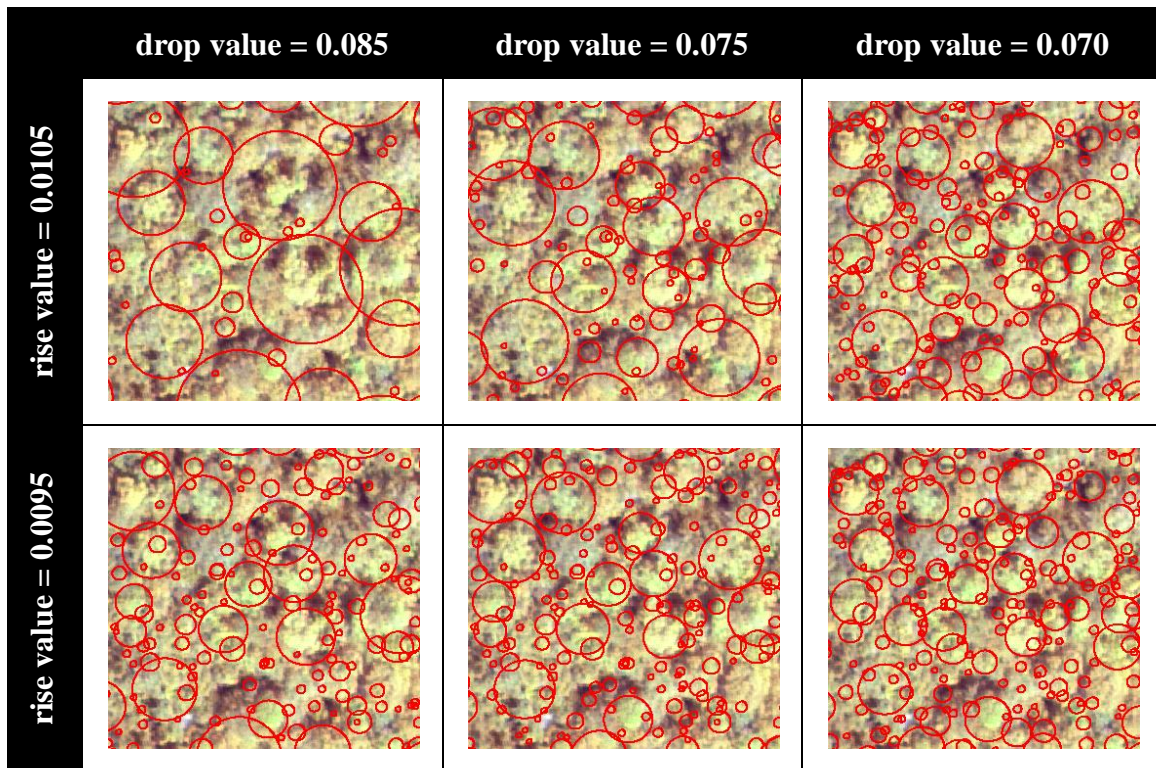
Table 7: Average diameter, maximum diameter and sample size associated with the two sites used for calibrating the crown delineation software. In this case, the software-based measurements are associated with the ultimate rise (0.0095) and drop (0.075) values used for analysis of the WorldView2 images.

	Measurement method	Average diameter (m)	Maximum diameter (m)	Number of trees
Closed canopy #2	In-situ	9.93	20.65	123
	DBH proxy (linear)	8.78	19.63	320
	DBH proxy (exponent)	8.34	17.92	320
	Software	5.54	31.98	1017
	Software (diameter > 4m)	8.84	31.98	474
Open woodland #1	In-situ	11.75	21.52	122
	DBH proxy (linear)	9.00	25.08	320
	DBH proxy (exponent)	8.57	21.20	320
	Software	5.44	35.14	596
	Software (diameter > 4m)	8.77	35.14	266

Table 8 illustrates how iterative adjustments to the rise and drop values contribute to visual changes in the locations and sizes of delineated trees. Scenes such as these were consulted during calibration to ensure that the program's approximations were realistically delineating trees. This table also demonstrates the tradeoff between calibration settings that overestimated the size of trees (drop value = 0.085, rise value = 0.0105) as compared to settings which

contributed to an overabundant delineation of subcrown areas such as individual boughs (drop value = 0.070, rise value = 0.0095).

Table 8: Comparison of the effect of several iterations of rise and drop values on the geometry of delineated trees. Each scene represents the same extent, with delineated crowns in red overlain on a pan-sharpened WorldView2 image.



Although the rise and drop values contribute significantly to the proper functioning of the crown delineation program, there are additional variables that can be adjusted to define the manner in which each image is analyzed. These include the smoothing window size, stop value, maximum transect length and minimum radius. As might be expected, the minimum radius limits the analysis to delineating trees that are larger than a certain threshold. In the case of this analysis, this was set to two pixels, which is equivalent to one meter. The maximum transect

length is somewhat the converse in that it sets a limit on the maximum length an ordinal transect can reach without being terminated. It is not, however, a limit on individual tree radii, as each radius is a summary of component transects. Thus, by definition, the maximum radius is necessarily some number smaller than the maximum transect length, which was set to 50 pixels, or 25 meters. In order to prevent transects from extending beyond the edge of the chip being analyzed, the maximum transect length also defines a border around each chip wherein no tree's centroid can exist. This boundary zone can be seen in figure 17 along the intersection of each chip.

The smoothing window size can be adjusted so that a more or less smooth image can be analyzed. In this case, a larger window size will contribute to a smoother image, by redefining each pixel based on a larger number of surrounding pixels. For the purposes of this study, the smoothing window size was set to its default value of 3 pixels across. The last value that was adjusted during the calibration of this software was the stop value. This variable is useful in terminating the analysis when the remaining unmasked maximum brightness value is equal to or less than the stop value. The justification underlying the stop value is that at a certain level of "darkness," either no more trees are left to be delineated, or they can no longer be done so properly. The drop value is set based on the difference between the mode and minimum pixel values divided by the difference between the maximum and minimum pixel values. Because some of the chips from the outside edges of the WorldView2 images contain blank areas with pixel values equal to zero, the stop value associated with these chips are also calculated to be zero. In order to ensure consistency across all chips and images, the stop value for the program was set to a static value of zero. In the case of inappropriate delineation due to this minimal stop value, the trees associated with the lowest peak brightness values could always be removed later,

contributing to the same results as if they were never delineated due to a higher stop value. This was not an issue, however, as the lowest peak brightness values were not associated with improperly delineated trees. Figure 19 highlights the bottom fifth percentile of peak brightness values and their associated tree approximations. It can be seen that this “darker” subset actually contains a number of appropriately delineated trees that would not be included had the stop value been raised.

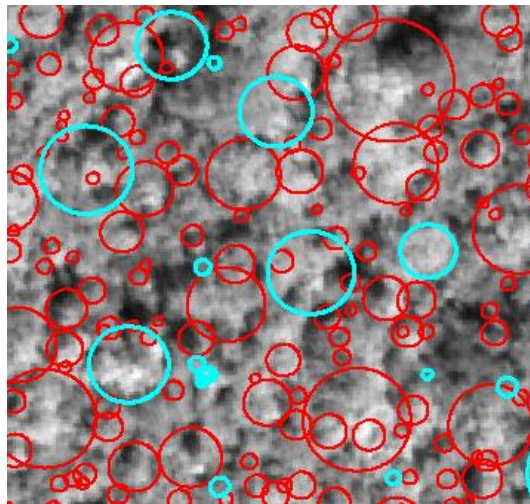


Figure 19: Circular tree approximations associated with a WorldView2 image analysis, where the trees with the bottom fifth percentile of peak brightness values are highlighted in teal.

3.5.2 Software analysis

After ideal calibration settings had been determined, the crown delineation software was used to analyze each of the 392 preprocessed chips. The output associated with this analysis was then imported into ArcMap and amalgamated into four appropriate datasets, one for each AOI for both image types. Figure 20 displays an example of the output from a scene within AOI1 as seen in ArcMap, where each tree is approximated by a red circle. The image on the left

represents the WorldView2 output overlain on the WorldView2 panchromatic image, and the image on the right displays the GeoEye1 output similarly on top of the GeoEye1 panchromatic image for the same geographic extent. Upon further scrutiny, it seems that there may be slight differences in the manner in which each of these images is analyzed, where the WorldView2 analyses tend to show a bias towards more, smaller diameter trees as compared to GeoEye1 analyses.

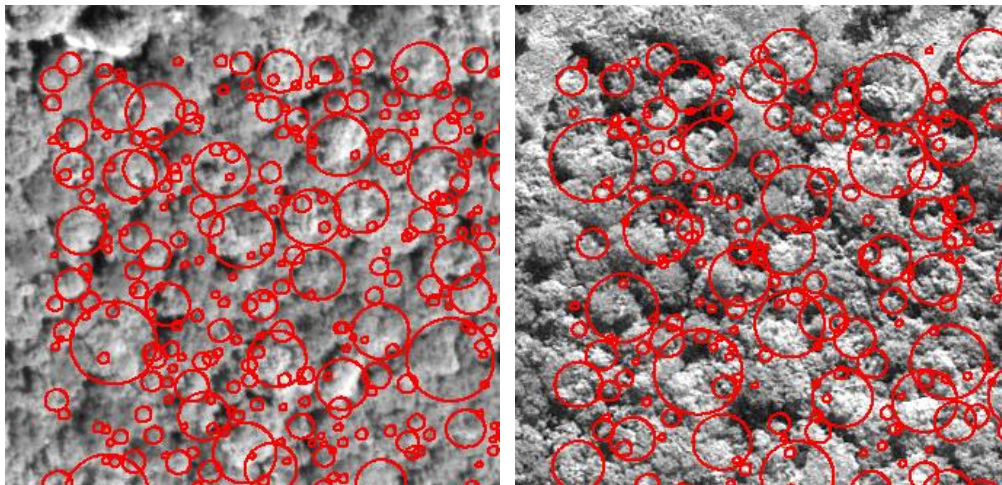


Figure 20: Raw output from the crown delineation software analysis imported into ArcMap. The image on the left illustrates a WorldView2 scene within AOI1, while the image on the right shows this same geographic area with its associated GeoEye1 output.

Figure 21 displays the cumulative distribution of tree diameters for each image analysis, grouped by area of interest. For both types of images, there is good agreement when comparing the cumulative distributions between each area of interest. Such agreement, however, is not extended to a comparison of the diameter distributions between each type of image. This

confirms the visual observation that the WorldView2-based analyses result in more trees of smaller diameters, whereas the GeoEye1-based analyses include more trees of larger diameters.

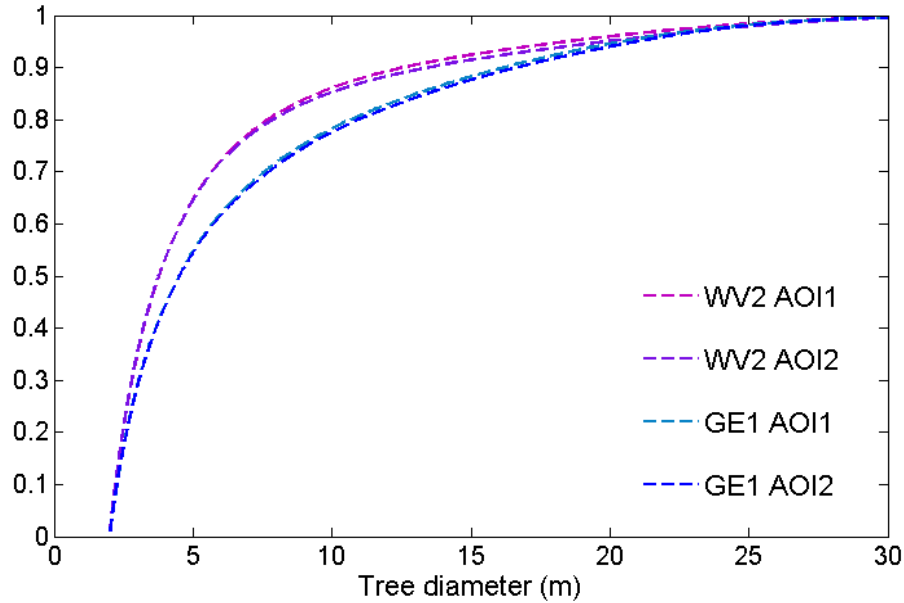


Figure 21: Cumulative distributions of tree diameters resultant from the software-based analyses of the four images associated with each of the image types and areas of interest.

In a separate calibration exercise, efforts were taken to adjust the aforementioned calibration variables such that the cumulative diameter distribution from the WorldView2 and GeoEye1 images more closely resembled each other. In addition to comparing these functions, the delineated diameters from each image were binned in one meter increments and compared as the GeoEye1 analysis was iterative adjusted. During this process, it became evident that a better fit between the analytical results of these two images was not possible, as either the upper, middle or lower bins could be appropriately matched, but not all three. Inconsistencies such as these highlight the difficulties inherent in comparing analyses rooted in two different datasets.

3.5.3 Results postprocessing

The results of the crown delineation analysis are critical in answering the hypotheses presented in section 2.1, but are not yet in a form that can robustly inform these questions. In order to disaggregate and refine the raw datasets outputted by the software analysis, a number of postprocessing steps are necessary. Essentially, the first step in postprocessing, was combining the individual chip outputs into the four main datasets as explained above. After that, the datasets can be grouped and groomed so that only the most relevant data remains.

The first step in grooming the datasets involved removing what were deemed to be “perturbed” areas. Such areas were demarcated if they contained confounding factors that could alter the way in which their pixels were analyzed by the crown delineation software. Figure 22 illustrates these areas, which include pixels marked by cloud cover, cloud shadows, significant anthropogenic development (including roads, buildings and clearings), pans and any null data areas. Most of these areas (such as clouds and roads) would be automatically masked and removed from the analysis due to the aforementioned NDVI filter. They were removed again during postprocessing for several reasons. The first is that this post-analytical method would allow for the removal of nearby, adjacent areas using a buffer. This is important for wispy, translucent areas around clouds that may not be removed by the NDVI filter in addition to the forested areas around roads, which would exhibit different characteristics than non-road adjacent forests. Additionally, this allowed for the spatial area associated with these unanalyzed pixels to be removed from the analysis area, contributing to a more accurate measurement of stem density. For this reason, the unanalyzed space between chips (due to the maximum transect length value) was also removed for its areal contribution. Both the WorldView2 and GeoEye1 images were demarcated with these designations, the combination of which was removed equally from both

datasets. Thus, even though the GeoEye1 images had zero cloud cover, the cloud and shade areas marked out in green and blue in figure 22 were still removed from this dataset. This was done in order to ensure a consistent area was being compared for both images.

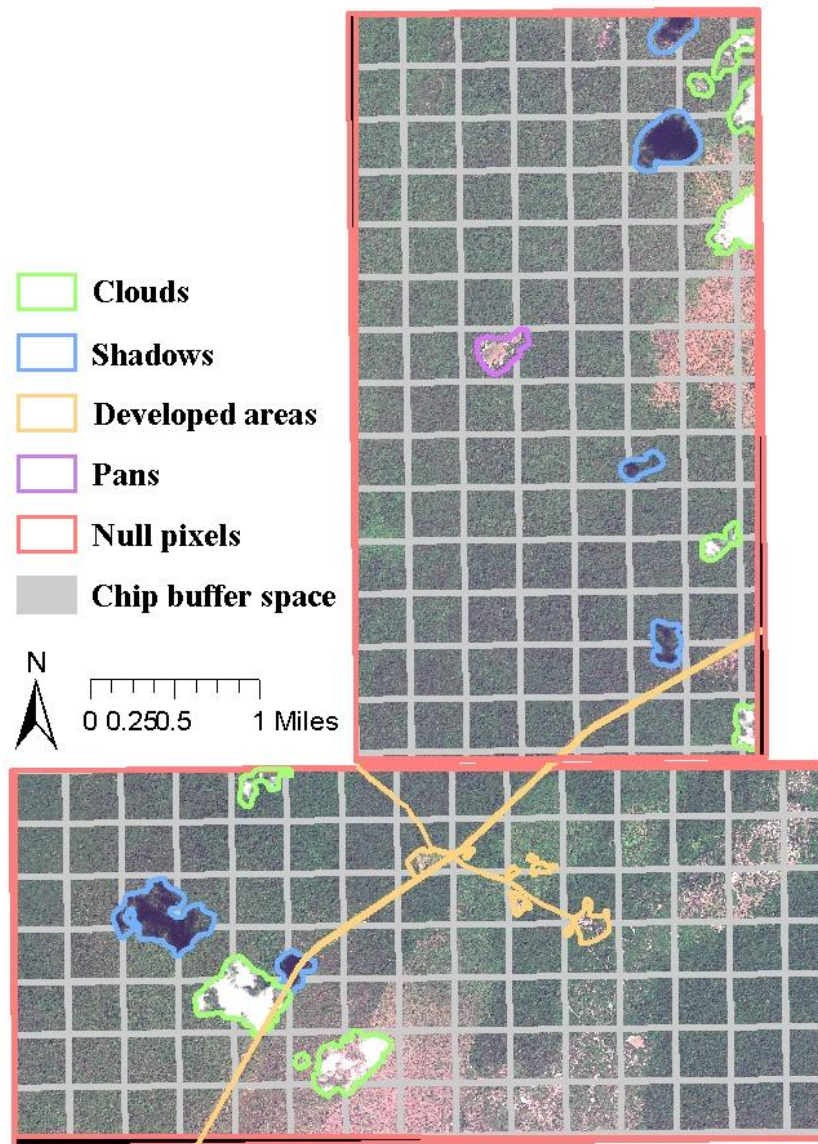


Figure 22: Illustration of the “perturbed” areas that were removed from each dataset overlaid on the WorldView2 images for each area of interest.

Once the perturbed areas were removed, the remaining data was grouped according to their block and forest type designations presented in figures 12 and 7. Additional sub-datasets were also created from the larger forest type classifications. The full transitional and open woodland datasets were broken into four geographically distinct regions. The EDM Limitada closed canopy area was also broken into three regions based on anticipated harvesting intensity. Each of these datasets was created in ArcMap by extracting those trees whose centroid fell within each classified area and grouping them together. Figure 23 displays how individual trees were grouped according to their location by block in AOI1. This figure also illustrates the absence of the perturbed areas as outlined in figure 22.



Figure 23: Tree crown delineation output for the WorldView2 AOI1 image, categorized and color-coded by block.

3.6 Numerical analysis

Upon completion of the requisite postprocessing steps, the refined datasets were imported into Matlab for a more in-depth analysis. Due to the nature of the output from the

crown delineation software analysis, the main metrics used in this analysis were average and maximum crown diameters, crown diameter distribution and stem density. The average and maximum values were fairly simple to compute for each sub-dataset using existing Matlab functions. Evaluating crown diameter distribution was less straightforward and was characterized through the use of cumulative distribution functions, histograms and the binning of tree diameters. Stem density was calculated by dividing the number of trees within each dataset by its area as calculated in ArcMap, while making sure to remove any areal contribution due to perturbed areas or the unanalyzed space between chips.

For reasons that will be discussed further in the section 4, this analytical step included additional postprocessing in the form of setting an iterative minimum tree diameter value. In order to disaggregate the contribution of the smaller tree approximations to stem density, average diameter and the distribution of tree diameters, supplementary datasets were created that removed these smaller trees. This was carried out in one meter increments from the default two meter minimum diameter through a 15 meter minimum length. This step serves a similar function as setting the minimum radius length variable during software analysis as described in section 3.5.1. The metrics discussed in the previous paragraph were similarly calculated for each of these auxiliary datasets.

3.7 Comparative analysis

One of the goals of this research is to provide insight into forest structure in a manner that would provide physical measurements and approximations of tree and forest properties. In addition, this research aims to provide insight into how a remote sensing analysis can prove to distinguish different types of forests based on their observable structure, patterns of disturbance

and/or anthropogenic land use. The benefit of a comparative analysis in conjunction to other analyses is the flexibility to focus more on similarities and differences between observations than on the quantitative meaning of measurements. Thus, even if a certain degree of geophysical accuracy is missing, the results of this study can be used to shed light on discernable and measureable differences between sites.

4 Results

The three research hypotheses presented in section 2.1 (1) address the relationship between remote sensing and in-situ data, and assess the utility of a remote sensing-based analysis in (2) detecting forest disturbance, as well as (3) identifying the relationship between forest structure and specific land management practices. The first of the hypotheses focused on the utility of a remote sensing-based tree crown delineation algorithm in identifying and measuring tree crowns in a manner consistent with field measurements and observations. An additional goal was to develop a method that was able to assess the range of land cover types found within this study's sites. Methodologically, this study will also determine whether the software analysis described above can provide accurate delineation and measurement of individual tree crowns utilizing high resolution WorldView2 and GeoEye1 images.

Evaluating the agreement between in-situ and remote sensing-based data relies on a complex calibration process conducted with the goal of verifying the utility of the crown delineation program (discussed in detail in section 3.5.1). The results of verification are summarized in table 7, which present the tree count, average tree crown diameter and maximum diameter of the calibrated remote sensing analysis along with results measured or derived from field observations. A subsequent post-calibration validation of alternative sites was also

conducted, the results of which are summarized in table 9. These values confirm that this study's methodology is yielding consistent results. Although these results are consistent, they are not necessarily reflections of precision or accuracy in delineation. Figures 19 and 20 illustrate the incomplete manner in which a subset trees are identified and demarcated. It can be seen that some trees seem appropriately delineated. Others tree approximations, however, represent overestimation in the merging of multiple crowns or underestimation by disaggregating a single crown into several smaller "trees". Collectively, these figures and tables shed light on the limitations in the methodology developed for this study. According to visual and numerical inspection, the results associated with relatively larger tree crowns seem to be effective representations of actual trees. Appropriate delineation at smaller diameters is less convincing, however. Figure 24 displays a WorldView2 scene overlaid with delineated trees that are distinguished based on their diameter. As can be seen on visual inspection, the larger red circles are more effectively delineating trees than the smaller circles in blue and green hues.

Table 9: Average diameter, maximum diameter and sample size associated with the two sites used for validating the crown delineation software. In this case, the software-based measurements are associated with the ultimate rise (0.0095) and drop (0.075) values used for analysis of the WorldView2 images.

	Measurement method	Average diameter (m)	Maximum diameter (m)	Number of trees
Closed canopy #1	In-situ	10.5	34.61	103
	DBH proxy (linear)	8.81	37.57	320
	DBH proxy (exponent)	8.21	27.38	320
	Software	6.11	33.16	1017
	Software (diameter > 4m)	9.93	33.16	474
Open woodland #2	In-situ	9.10	18	121
	DBH proxy (linear)	8.73	16.04	320
	DBH proxy (exponent)	8.35	15.41	320
	Software	5.80	35.36	899
	Software (diameter > 4m)	9.09	35.36	431

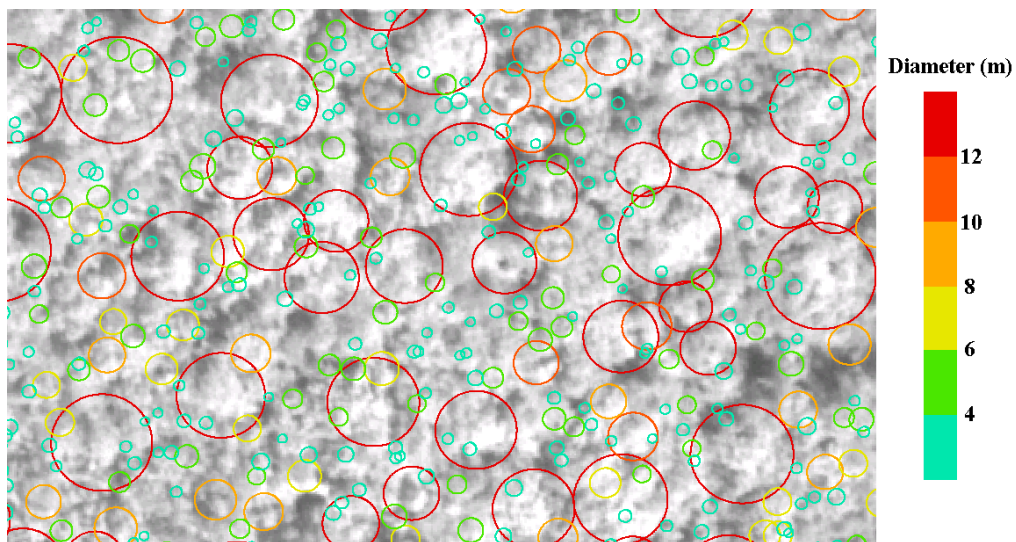


Figure 24: A WorldView2 panchromatic scene with various tree crown approximations color-coded according to their diameter.

Additional questions regarding the accuracy of crown delineation are raised by the diameter distribution variation between WorldView2 and GeoEye1 images as presented in figure 21. Some divergence is to be expected due to temporal variations, since these images were captured two and a half years apart. However, this level of deviation is sufficiently large to suggest that this is a function of the manner in which each image is analyzed, as opposed to a reflection of actual forest structure change. Because of the questions regarding the accuracy with which trees of diameters less than ten meters are delineated, the first hypothesis can neither be confirmed nor denied. However, the software-based analysis, when viewed independently of the accuracy of delineation, seems to provide consistent analysis across a range of forests from dense, closed canopies, to sparse, open woodlands. Figure 27 illustrates the consistency with which various subplots were analyzed using the tree crown delineation software. This figure also presents further evidence of the inconsistencies between WorldView2 and GeoEye1-based analyses. As such, the results from each of these types of images will be considered separately in subsequent discussions.

Because this software-based analysis did not produce effective delineation, the existing dataset was modified by removing the influence of smaller trees and creating supplementary datasets as described in section 3.6. These modified datasets were subjected to subsequent analysis focused on the larger subset of delineated trees, which reflect a more appropriate characterization of forest structure. Upon visual inspection, it is apparent that the accuracy of individual tree approximations generally decreases as tree diameter decreases. It seems likely that these smaller trees are misrepresentations of subcrown canopy areas such as boughs. The systematic removal of these smaller “trees” from subsequent datasets also removes the influence

of that portion of the canopy. This will necessarily lead to undersampling, a caveat that is noted in subsequent analyses.

After comparing minimum tree diameter thresholds numerically and visually, an eight meter diameter was set as the most appropriate cutoff. This value balances the influence of inappropriately delineated trees, with that of undersampling due to the removal of small but appropriately marked trees. This is illustrated in Figure 24 which includes those trees that meet this threshold demarcated in red and orange, and excludes those marked in yellow, blue or green. Figure 25 displays tree diameter cumulative distribution functions for each image type and AOI after the trees with diameters less than eight meters were removed. This graph stands in stark contrast to figure 21, which includes a full dataset of trees with no minimum threshold. The difference in diameter distribution which is obvious between image types in figure 21 is barely noticeable in figure 25. Thus, applying the eight meter threshold provides a consistent dataset for comparison across image types. Subsequent discussion will evaluate results both inclusive and exclusive of this threshold.

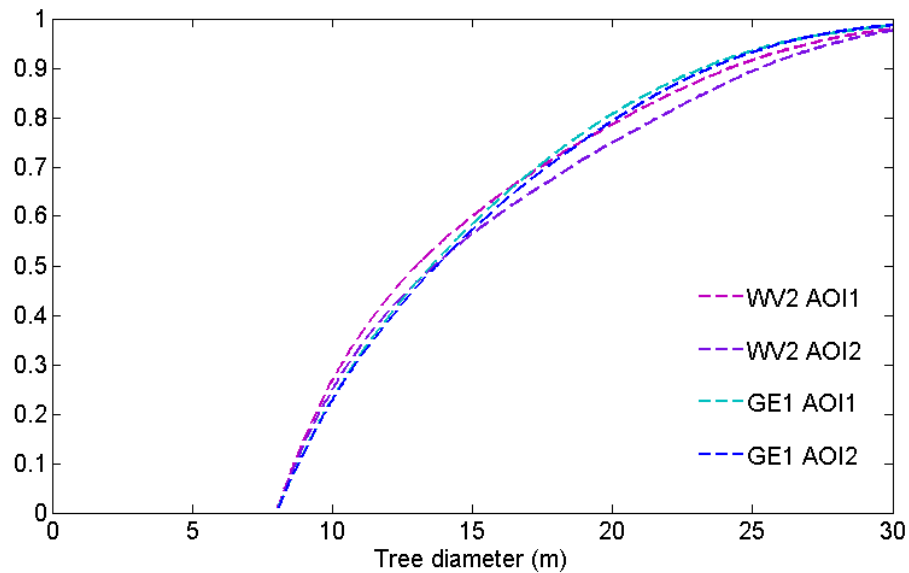


Figure 25: Cumulative distributions of tree diameters greater than eight meters as determined by the software-based analyses of the images associated with WorldView2 and GeoEye1 payloads for each area of interest.

The second and third hypotheses presented in section 2.1 focus on the link between forest structure and disturbance regime. In particular, these two hypotheses express an interest in connecting observable dissimilarities in forest structure with the anthropogenic activities associated with those forests. In this study, which is centered on two forestry concessions, forest disturbances are related primarily to lumber harvesting operations. These hypotheses suggest that differences in harvesting operations will be detectable by analyzing high resolution remote sensing images with an automated crown delineation software. The results of these analyses support the hypothesis that differences in forest structure can be detected by a crown delineation algorithm. Whether these differences are due to underlying anthropogenic activity, however, is less clear. This limitation appears to be more a function of limits in temporal comparison analysis than errors or shortcomings associated with the crown delineation software.

In the areas studied, differences in tree size distribution, average crown diameter and stem density could be a reflection of anthropogenic disturbances, natural variation in forest characteristics due to a broad set of environmental variables, or a function of both. The range of forest types within each study site highlight the degree of variability in forest structure that is introduced due to natural variation. Thus, it becomes difficult to identify the more subtle changes in forest structure that could be characteristic of anthropogenic influences. Temporal comparisons can help differentiate between natural variations and those resultant of disturbances by providing a baseline with which to compare changes over time. Typically, significant changes over a short period of time are more likely due to anthropogenic activity. That being said, climatic and environmental factors (such as drought, flooding, fire, etc.) can also have significant effects in the short term. However, these natural phenomena are likely to be known events facilitating accurate differentiation between these and changes due to human activity. Thus, inclusion of repeat measures of temporal datasets interpreted in conjunction with known climactic events should lead to increased confidence in the designation of the cause of variation in forest structure. For this reason, two datasets spanning two and a half years were used for this study. Unfortunately, because of the limitations in data availability (as discussed in section 3.2), these datasets come from two separate satellite payloads, which does not allow for effective cross-comparison. This in turn led to the inconsistencies reported in section 3.5.2. Because these two datasets cannot be properly compared, the robustness of temporal analysis is undermined. This limits the extent to which hypotheses two and three can be evaluated. However, meaningful distinctions were noticed, particularly in the WorldView2-based analysis, which will be discussed in further detail.

As alluded to above, it is important to characterize a baseline or “natural state” of terrestrial surfaces before attempting to interpret the impact of human-induced changes. The term, “natural state” is somewhat misleading, given that forest ecosystems are constantly changing in response to an array of environmental stimuli. That being said, if considered on relatively small time scales, it can be assumed that most changes to this natural state are due to anthropogenic activities or other large-scale disturbances (such as natural disasters, infestations, etc). In recognition that forests are constantly changing, the natural states within this study’s areas of interests were defined by three broad categories: closed canopy forests, open woodlands, or intermediate semi-closed canopy forest (see figure 7). It should be noted that these more classifications as demarcated with the help of the TCT Catapu management and field observations vary significantly to the coarser scale classifications presented in figure 5.

Given these predefined classifications, this study was well-positioned to evaluate the ability of a tree crown delineation analysis to provide insight into land cover classifications. To test whether this type of analysis can indeed help with classification, it is necessary to assess whether a significant distinction between forest types can be recognized. Using the metrics discussed previously (diameter distributions, average diameter and stem density), several woodland and closed canopy datasets were compared for their relative differences. These subsets included the four previously-classified woodland regions and all eight TCT Catapu management blocks that fell entirely within the closed canopy areas as illustrated in figure 26. The respective cumulative diameter distributions for each of these subsets (and their aggregated sum) are displayed in figure 27. As discussed previously, these distributions are evaluated with and without the eight meter minimum diameter threshold and for both WorldView2 and GeoEye1 images.

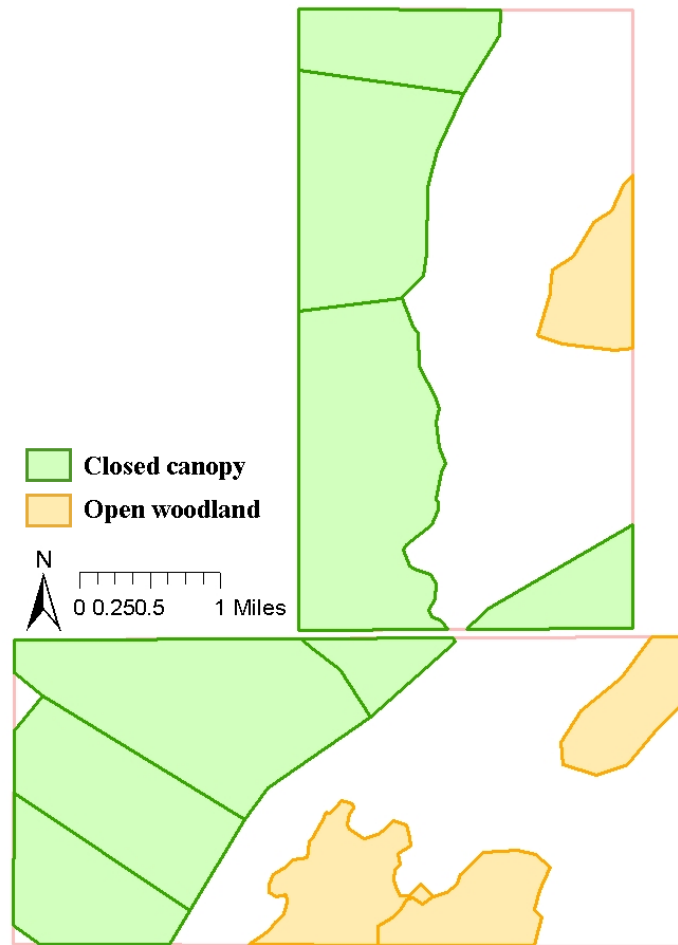


Figure 26: Illustration of the four woodland and eight closed canopy subset used for comparative analysis.

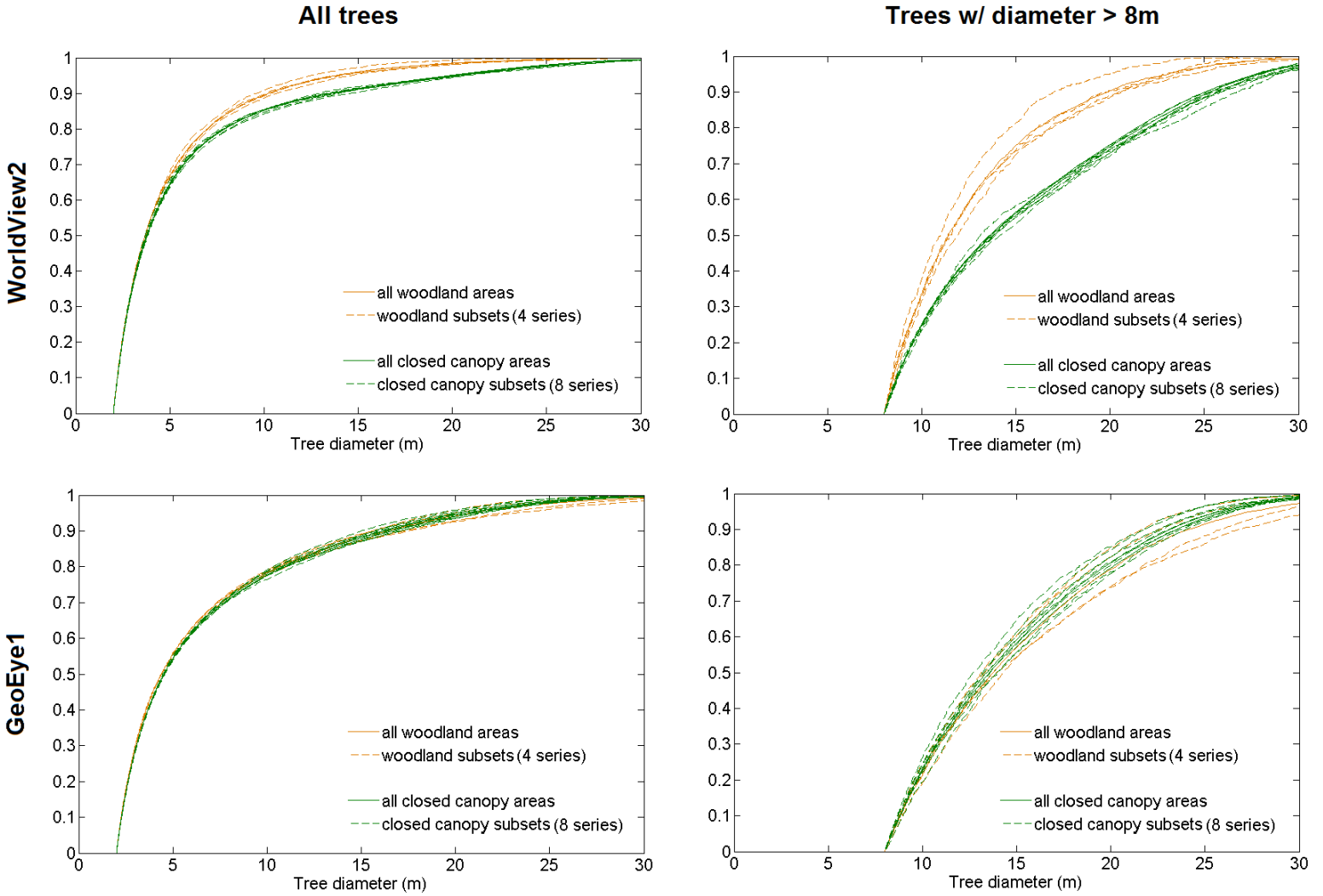


Figure 27: Cumulative diameter distribution functions for woodland (orange) and closed canopy (green) areas. Each subset is marked by a dashed line, while the aggregated sum for each type of forest is represented by a solid line. The four graphs compare the WorldView2 and GeoEye1 analyses for all tree crowns contrasted with a subset containing only those trees greater than eight meters in diameter.

The graphs above provide mixed evidence for the effectiveness of using a crown delineation analysis for distinguishing among forest types. In the case of the WorldView2-based

analysis, there seems to be a clear, consistent and significant difference between open woodland and closed canopy areas. Woodland areas have a steeper initial incline, representing the presence of more trees of an intermediate size (between about 8 and 15 meters in diameter) and relatively few very large trees (greater than 25 meters in diameter). The closed canopy subsets exhibit a more even distribution among intermediate and large trees as suggested by the more constant slope among trees greater than about eight meters in diameter. As discussed previously, the uncertainty inherent in this analysis does not necessarily mean these distributions represent the reality present on the ground. The more consistent diameter distributions seen in the closed canopy areas may in part be a reflection of a greater number of merged and overestimated trees as compared to woodland areas. Tree crowns are more likely to be merged or overestimated when the edge of the crown is not marked by significantly different pixel values. This, in turn, is more likely to occur in closed canopy areas, where a consistent canopy represents a more homogeneous surface than the intermittent bare soil and grasses present in woodland areas. Regardless of the reasons behind these distributions, it does prove that there is a measurable and noticeable difference in the way that woodland and closed canopy areas are delineated when using a WorldView2 image. Including the diameter distributions of intermediate semi-closed canopy forests as in figure 28 provides consistent results, as well. The distributions associated with these datasets fall somewhere in between closed canopy and woodland distributions, as would be expected. When viewing the results of the GeoEye1-based analysis, however, any distinction breaks down. Whereas the woodland and closed canopy distributions for the top two graphs in figure 27 clearly diverge, they are essentially overlapped in the bottom two, GeoEye1 images. As such, a GeoEye1-based crown delineation analysis (as calibrated according to this study) cannot be used to confidently distinguish between different forest types.

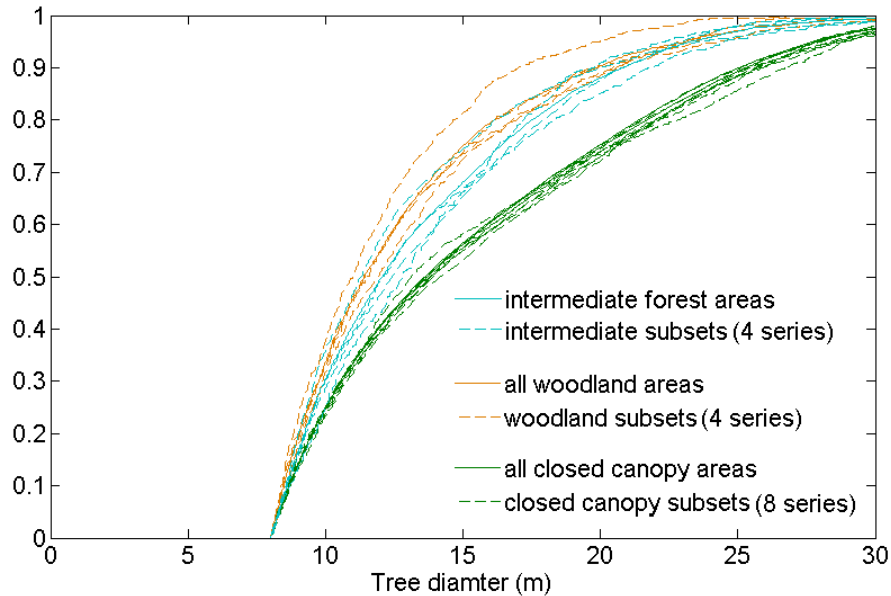


Figure 28: Cumulative diameter distribution functions for open woodland, semi-closed intermediate and closed canopy areas. The results are based on a WorldView2-based analysis and the inclusion of an eight meter diameter threshold.

Comparing these same datasets according to their stem density and average tree diameter provides additional metrics with which to view any dissimilarity among forest types. Figure 29 displays these values for each area according to image type and diameter threshold in a manner similar to figure 27. Figures 30 and 31 illustrate the differences in these metrics among the various sub-datasets for a WorldView2 based analyses with an eight meter diameter threshold (additional graphics for GeoEye1 images and those without a threshold are included in Appendix C). The results apparent in these scatter plots and graphics confirm the conclusions drawn in the previous paragraph. Again, there is a clear and significant distinction between the woodland and closed canopy areas when comparing the WordView2-derived results. The analyzed woodland areas are characterized by notably smaller stem densities and average diameters as compared to

the closed canopy areas. The GeoEye1-based results exhibit a lack of this obvious distinction, though a slight variation is evident. As with the WorldView2 results, the woodland areas tend to exhibit smaller stem densities, as would be expected in a forest type that is characterized by fewer trees and more open areas. There is not a noticeable difference in the average tree diameters associated with each forest type for GeoEye1-based results. In all of the aforementioned cases, the exclusion of trees under eight meters in diameter serves to increase the evident distinctions between subsets. This makes sense because of the relatively similar distribution of trees below this threshold across subsets.

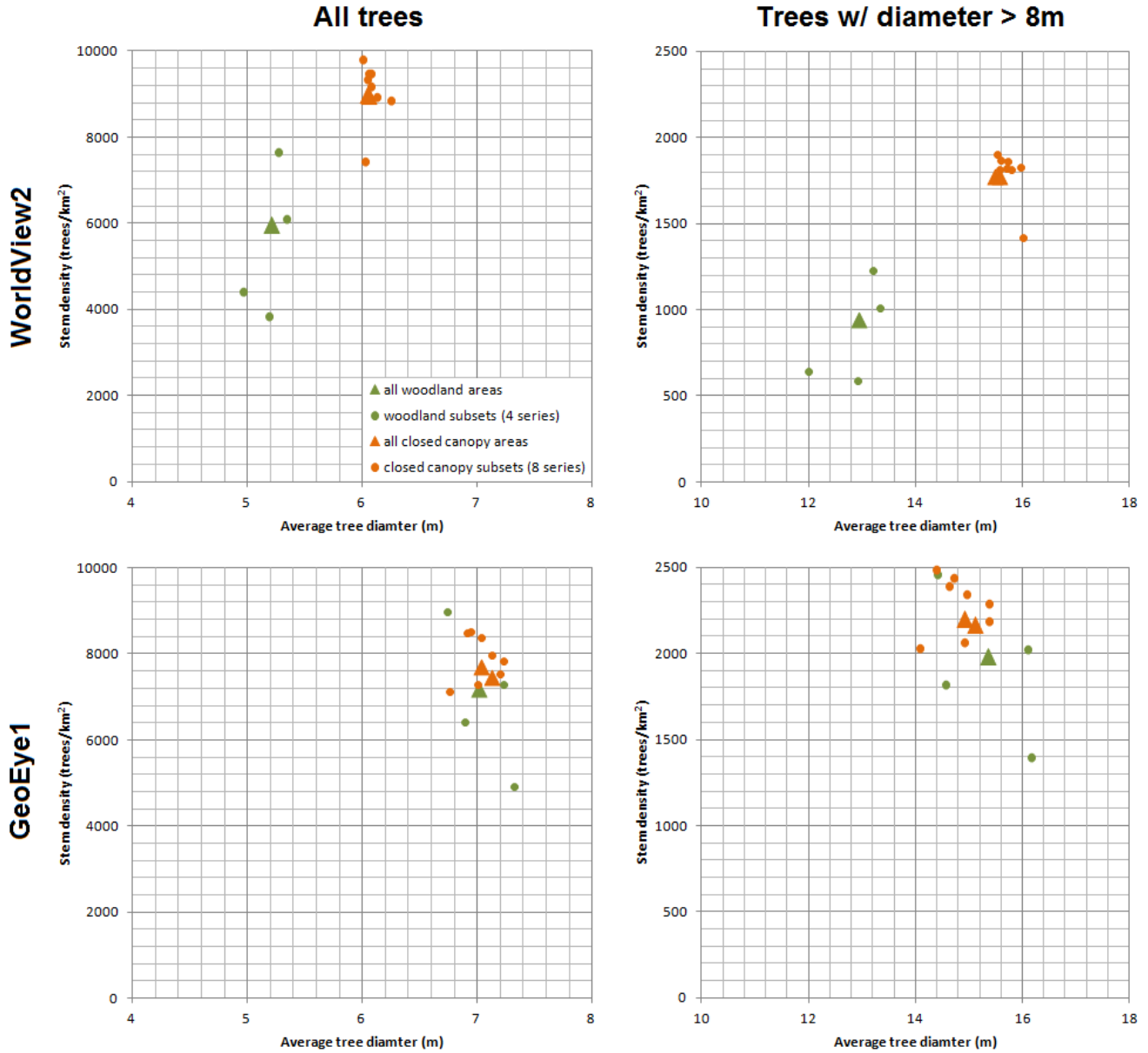


Figure 29: Scatter plots comparing average tree diameter and stem density for woodland (orange) and closed canopy (green) areas. Each subset is marked by a circle, while the aggregated sum for each type of forest is represented by a triangle (the two orange triangles represent each AOI). The four graphs additionally highlight the differences between WorldView2 and GeoEye1 analyses and due to the inclusion of an eight meter diameter threshold.

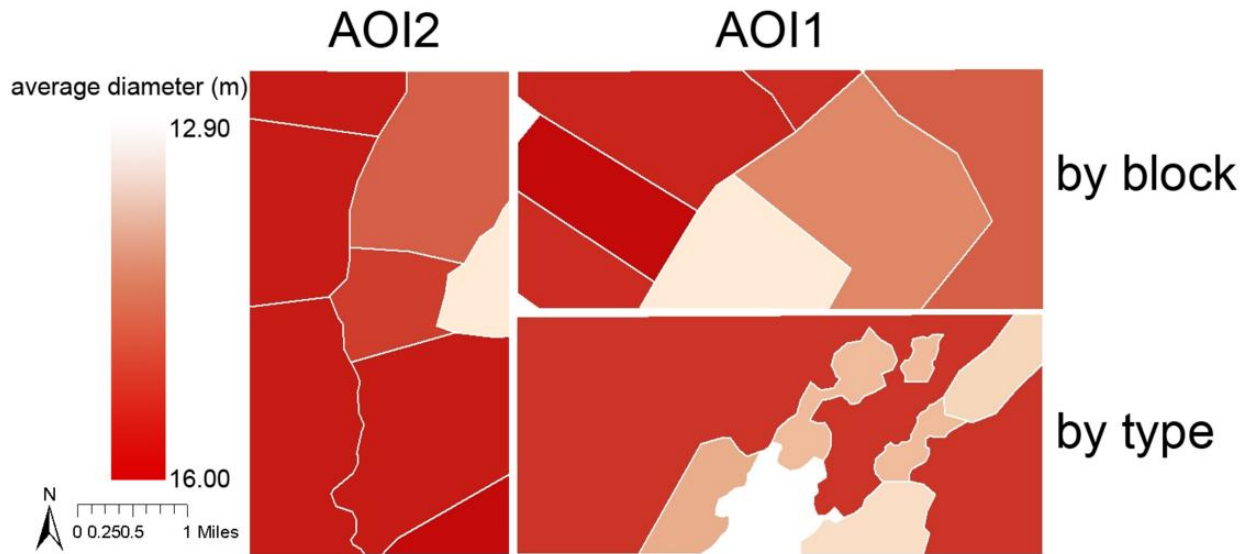


Figure 30: Geographic illustration of each sub-dataset in the WorldView2 analysis according to their mean diameter value. These values reflect the inclusion of an 8 meter diameter threshold.

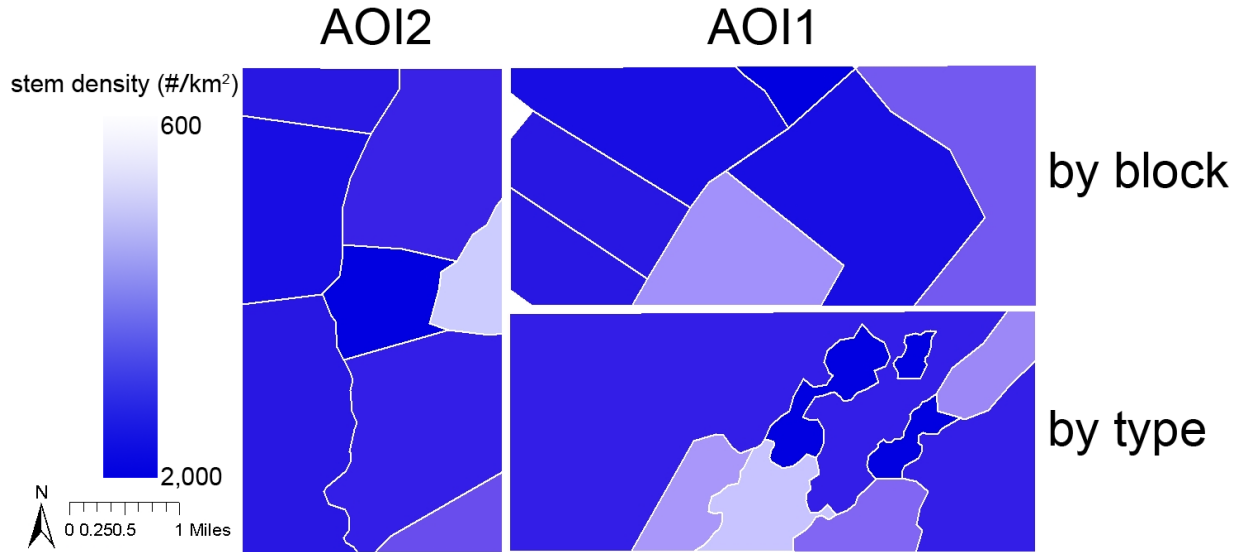


Figure 31: Geographic illustration of each sub-dataset in the WorldView2 analysis according to their stem densities. These values reflect the inclusion of an eight meter diameter threshold.

For the reasons set forth above, temporally distinct datasets are necessary for a robust analysis of the effects of anthropogenic activities on forest structure. Unfortunately the temporally varied datasets in this study (represented by the baseline GeoEye1 image and the more recent WorldView2 image) exhibit very little consistency and cannot be appropriately compared. Additionally, the GeoEye1 dataset as a whole provides very little insight into the variations in forest structure present within this study's areas of interest. Ideally, this dataset would have described a certain baseline scenario with which to compare the known harvesting activities presented in sections 2.2 and 3.1. Since this is unavailable, certain assumptions were necessary for an evaluation of the link between forest structure and harvesting disturbances. Of these, the most significant is that the areas to be compared (which include most of the closed canopy area in AOI2) are assumed to have been essentially similar in structure prior to any anthropogenic disturbances. Therefore, any noticeable variations among these areas are assumed to be reflections of the manner in which each of these areas was harvested. The TCT blocks in this comparison were harvested from 2001 to 2006 (table 3), while the EDM concession was harvested between 2009 and 2012. The EDM concession area was broken up into three sections according to harvesting intensity level, which are displayed in figure 32. EDM central is characterized by having experienced the most intensive disturbances associated with logging activities, followed by EDM north and EDM south. In order to further remove any influences due to spatial variation, approximately equal areas on either side of the TCT-EDM border were also compared for variability. These areas were created by generating a 500 meter buffer on each side of the border and removing the unforested pan in the middle. The trees whose centroid fell within either the TCT or EDM buffered area were aggregated into a dataset for subsequent analysis. These buffer zones can be seen in figure 32.

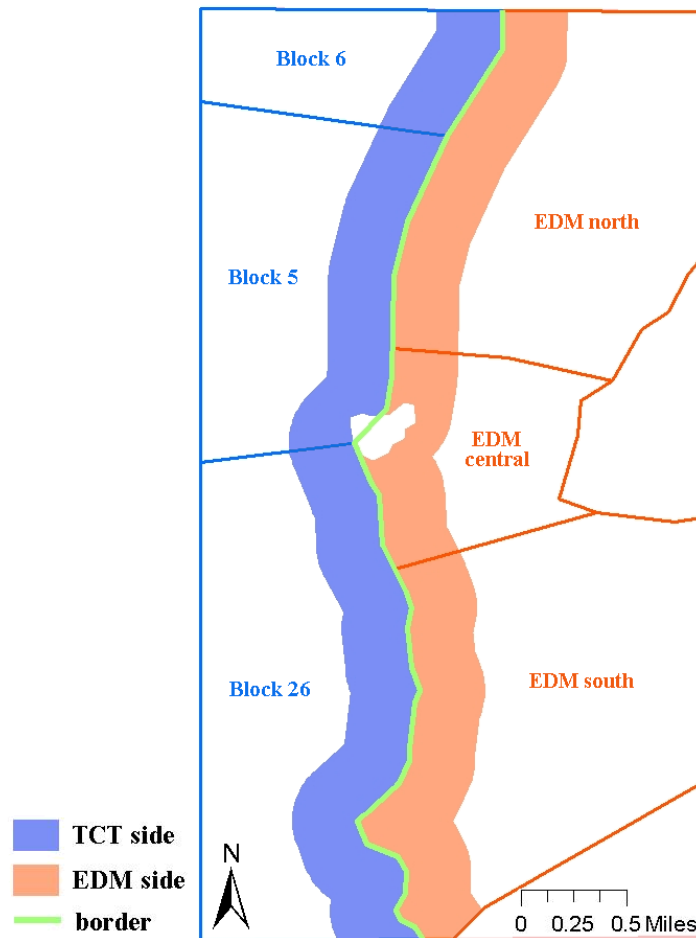


Figure 32: Map of AOI2 that illustrates the three TCT blocks and three EDM areas that were used to compare the link between forest structure and harvesting method. The 500 meter buffer zone on either side of the border is also displayed and color coded according to concession.

The subsets within each concession displayed in figure 32 were compared based on their average diameters and stem densities in a manner similar to figure 29. The resultant scatterplot can be seen in figure 33. Upon viewing these scatterplots and the graphic representation in figure 31, there is not a clear distinction among the stem densities associated with each concession area. When comparing average densities, however, the EDM Limitada areas exhibit generally smaller

values (and lighter shades in figure 30). As would be expected, the more intensely harvested EDM north and EDM central subareas exhibit the most noticeable differences. Figure 34 illustrates diameter distribution differences among the EDM north and central subsets as compared to the TCT Catapu blocks. In all such comparisons, these two subsets exhibit qualities (such as a smaller average diameter or the presence of more intermediate sized trees) that characterize a shift away from a closed canopy state towards more of an open woodland state. This is a logical shift for an area that has experienced significant disturbances wherein many trees have been felled for lumber harvesting.

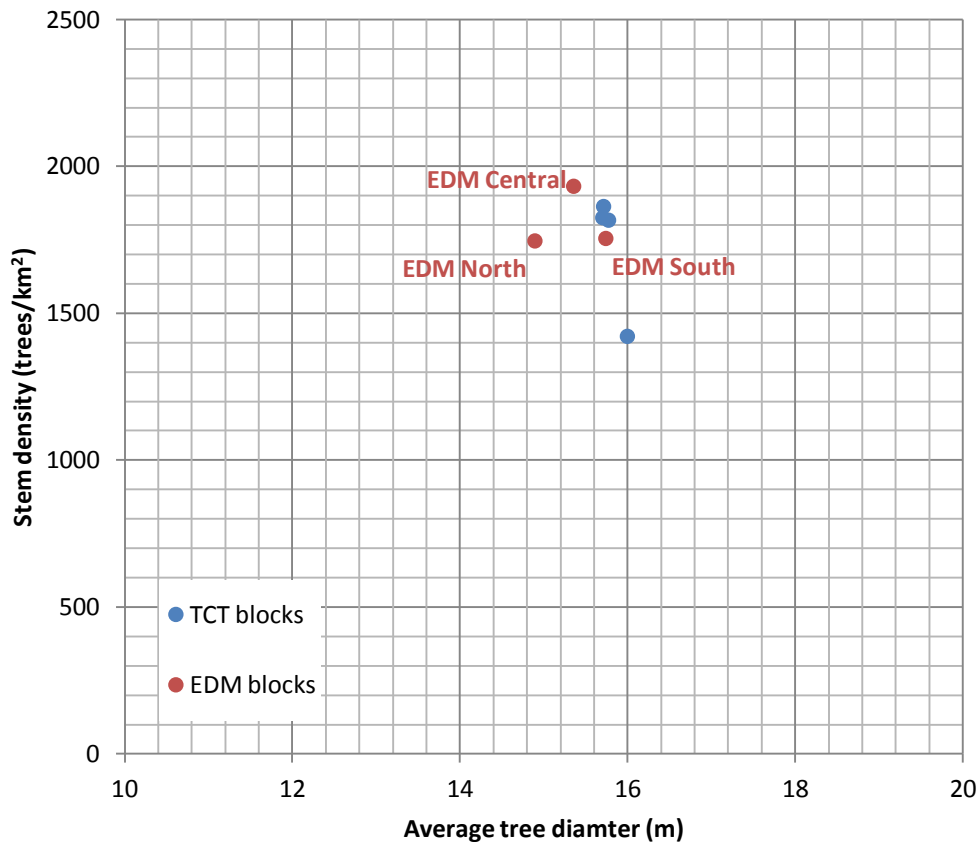


Figure 33: Scatter plots comparing average tree diameter and stem density for TCT Catapu (blue) and EDM Limitada (blue) areas. These results come from the evaluation of datasets with an eight meter minimum diameter threshold.

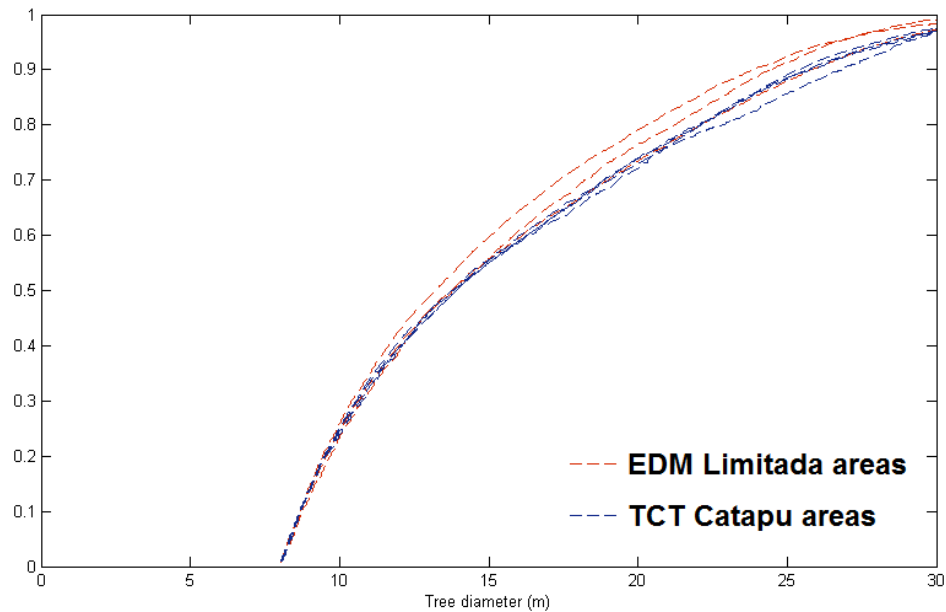


Figure 34: Cumulative diameter distribution functions for subareas within the EDM Limitada and TCT Catapu concessions. The results are based on a WorldView2-based analysis and the inclusion of an eight meter diameter threshold.

The results of a comparison of each buffer zone according to average diameter and stem density are summarized in table 10. These values provide further evidence that what should be two statistically similar areas, in fact exhibit dissimilarities in forest structure. Applying a t-test to the buffer datasets on either side of the TCT-EDM border confirmed that the EDM population of diameters is significantly smaller than the TCT population with a p value of less than 0.0015. This provides further evidence that forests within the EDM concession are displaying evidence of the more intense disturbances that they experience. The feasibility of utilizing a tree crown delineation analysis to link forested areas with their harvesting schemes cannot be conclusively

proven because of the lack of a reliable baseline for comparison. That being said, the evidence set forth in this section suggests that this may be a plausible application of such an analysis.

Table 10: Average diameter and stem density of the trees within each 500 meter buffer zone on either side of the TCT-EDM concession border. Included are these values with and without the inclusion of an eight meter diameter threshold.

		TCT side	EDM side
all trees	average diameter (m)	6.108*	6.049*
	stem density (trees/km ²)	11716	11916
diameter > 8m	average diameter (m)	15.791	15.553
	stem density (trees/km ²)	2339	2366
			* p < .0015

5 Discussion and Significance

Although the study hypotheses were not confirmed, a number of valuable insights can still be drawn from the results of this research. These insights are based on the use of a tree crown delineation software suite as a tool for comparative analysis as opposed to a tool for complete and accurate measurement of individual tree crowns. This software-based approach has proven to be a successful measurement tool in the past, but not in this particular study. This could be due to several reasons. The untested nature of the WorldView2 and GeoEye1 systems used in this study present the possibility that the datasets are not sufficient to allow for a proper analysis. The inconsistency between the results of the WorldView2 and GeoEye1 analyses are particularly telling in this regard. It suggests that the manner in which crowns are delineated can be a function of the input image, and thus that analytic methods would need to be customized to specific image acquisition systems. It is also possible that elements such as sun angle and satellite angle off-nadir (which were not measured in this study) affect the influence of canopy

shadows within images. This would in turn affect the manner in which images are delineated, as shadows tend to facilitate the terminating of transects. The utility of these types of datasets might also be improved with further preprocessing steps, such as the inclusion of atmospheric and solar gain corrections, or by an adaptation to the smoothing window. The nature of the site itself and the forest structure present on the ground could also introduce a number of confounding characteristics not present at other more effectively-delineated sites.

Regardless of the limitations in the geophysical accuracy of this methodology, the results point to several important applications for this type of research. Based on the comparative analyses discussed above, this type of crown delineation analysis could be useful in regional scale land cover classification. The WorldView2 analysis was particularly effective in distinguishing open woodland and closed canopy type forests. Thus, depending on the presence of a minimum diameter threshold, a classifying algorithm could be developed to aid in the delineation of various forest and non-forest ecosystem types. Classification algorithms are already an established tool for distinguishing among land cover type. Typically, the algorithms rely on numerical comparisons and ratios among the bands of a multispectral image (Foody G. M., 2002). The results of this study suggest that incorporating structural aspects into these classification schemes will lead to increased accuracy. Many of these algorithms use decision trees that proceed through a number of comparative steps before arriving at an estimated land cover type (DeFries & Chang, 2000). The results of a crown delineation analysis could easily be incorporated into existing characterization methods. Table 11 presents two schemes that could be used to distinguish woodland and closed canopy areas within the study sites for a WorldView2-based analysis.

Table 11: Example classification schemes for the WorldView2-based analysis of forested areas within this study’s site. A dataset that meets the inequalities present in this table can thusly be designated as either woodland or closed canopy forest, where S is stem density in trees/km² and D is average diameter in meters.

diameter threshold	woodland	closed canopy
none	$S < 8000 \ \& \ D < 5.5$	$S > 7000 \ \& \ D > 5.9$
8 m	$S < 1300 \ \& \ D < 14$	$S > 1300 \ \& \ D > 15$

The classification techniques discussed above can also be effectively applied to monitor forest changes in response to anthropogenic disturbances. The results presented in figures 30, 33 and 34 and table 10 show the sensitivity of this study’s analysis to subtle changes in forest structure due to harvesting regimes. The datasets associated with harvesting within the EDM Limitada and TCT Catapu concessions exhibit a distinct pattern of contrast, which is consistent with the observed status of EDM Limitada as a more degraded forest. Unlike in some regions where deforestation is easily visible at high resolutions, forest degradation due to overharvesting in the study’s region is less obvious. This appears to be a function of the relatively large number of noncommercial tree species that are left unharvested, resulting in a forest that continues to appear in a “closed canopy” state. Because the study methodology is sensitive to change of this type, it can serve as a tool for agencies interested in detecting and monitoring forest degradation due to harvesting practices. However, this would require a temporally distinct baseline condition with which to compare such changes. While there are limitations in the sensitivity of this approach, it can be a very useful tool in pinpointing areas of likely degradation which can then be subject to further study.

Further adjustments in this study's methodology that contribute to more effective delineation could introduce additional applications such as above ground biomass estimations and monitoring of carbon stocks over larger spatial and temporal scales. Although this study was not sufficiently precise in the delineation of tree crowns to calculate a confident estimate of biomass, the allometric equations derived in section 3.3 offer a pragmatic starting point for subsequent estimates of biomass for this region.

This research contributes an incremental step in developing remote sensing techniques for monitoring and measuring forest ecosystems. Although some results are inconclusive, this study has proven the feasibility of remote sensing in the analysis of forest structure in the Dry Deciduous Lowland Forests of Mozambique. This study also provides an assessment of the strengths and weaknesses of a particular methodology applied to this unstudied forest type. In addition, this study offers a resource for subsequent research initiatives interested in measuring forest structure.

5.1 Supplemental Research Suggestions

The use of untested remote sensing images in this study's analysis leaves several questions unanswered. Namely, whether the type of images was a contributing factor in the incomplete manner in which individual trees were delineated. As such, it would be useful to apply the same methodology to Ikonos and/or QuickBird images for a similar forested area. This would provide insight into whether the limitations in the current study are derivative of the image type, a function of the methodology, or perhaps due to some other factor.

The successive analysis of multiple, additional WorldView2 and GeoEye1 images across time would reveal whether the limitations in the methodology diminish across repeat trials to a

sufficient degree to provide a more effective tracking of forest change. As both of these satellite payloads are still in operation, there is a good chance that additional images for these AOIs will become available. The opportunity for additional analysis of multiple images of the same type for these study sites might be revealing in regard to the link between harvesting disturbance and forest structural response. Unfortunately, however, these images will not be useful in providing any additional insight into the state of the EDM Limitada concession prior to its intensive harvesting episodes beginning in 2009.

Since images from the same satellite payload will not always be able to be compared, it would be useful to introduce more consistency across image types. One way to do this could be the reintroduction of atmospheric and solar gain corrections into the preprocessing code for WorldView2 and GeoEye1 images. This would require that certain calculation and coefficients need to be established, which would ideally contribute to preprocessed images that are more consistent across types. Additional methods could involve adjusting the smoothing filter based on image type due to varying radiometric variability, or introducing other normalization schemes.

It would also be useful to examine the potential use of publicly available high resolution imagery for this type of analysis. These could include images from Google Maps, Bing Maps, or ESRI World Imagery. Although this type of analysis would not allow NDVI masking due to the absence of multispectral bands, a method incorporating these datasets could significantly reduce the financial burdens associated with purchasing high resolution images.

The analysis employed in this study is limited by tradeoffs inherent in spatial versus temporal resolution, as well as by the cost associated with data acquisition and analysis. Because fine-scale images are costly in terms of time and finances, there is a growing interest in pairing

fine-scale analysis with coarser-scale remote sensing products in order to evaluate larger swaths of land over more frequent intervals. It has been suggested that coarse (MODIS or MISR) to medium-scale (Landsat) datasets be used to extrapolate fine-scale analyses over larger areas in order to marry the precision associated with fine-scale analysis with the scope of coarser datasets, (Hansen, et al., 2008; Frohling, et al., 2009). Applying finer-scale analyses to broader extents has shown some success in leveraging coarser-scale analyses to pinpoint areas for fine-scale study (Hansen, et al., 2008; Asner G. , 2009; Tomppo, Nilsson, Rosengren, Aalto, & Kennedy, 2002). This research could similarly stand to benefit from an extrapolation technique that could increase the temporal and spatial extent to which these analyses could be applied.

6 Acknowledgements

Throughout the course of this research project, several mentors and collaborators stepped forward to contribute above and beyond the call of duty. While on the ground in Mozambique, James, Pat and Graeme White were absolutely instrumental in ensuring a safe and productive research experience. As managers of the TCT Catapu concession, they expressed a constant willingness to help, sharing their limited time and resources to make this research a priority in their busy schedules. As collaborating partners, they shared invaluable knowledge with regards to countless topics especially as they pertained the specifics of the flora, fauna, economics, demographics and politics of the areas where this research is centered, all the while exhibiting hospitality and transparency into their operations. As friends they provided lodging, food and travel as well as connections to fellow researchers, practitioners and travelers that could contribute to this research. Additionally, TCT Catapu employees, David Peter and Domingos Mozinho were influential in ensuring a safe field environment, warding off various undesirable

reptiles, arachnids and arthropods, while contributing to efficient measurements and providing tree designations for hundreds of different species.

Ivan Remane was another selfless and invaluable member of this research endeavor. As a graduate student, knowledgeable in forestry, especially as it pertains to Mozambique, he provided constant mentoring and feedback from the inception of this research through every aspect of its implementation. He was willing to contribute such knowledge remotely from Southern Illinois University or in-person as he accompanied the field expedition, travelling thousands of miles and braving the humid, dense forests of Sofala for several weeks in June. This research would absolutely not have been possible without his help and the additional advising and flexibility of his advisor, Dr. Matthew Therrell.

Last, but certainly not least, are the innumerable contributions shared by committee members, Dr. Robert J. Swap, Dr. Jennie Moody, Dr. Michael Palace and Dr. Hank Shugart. Each and every one of them was willing to spend countless hours guiding this research and contributing to an invaluable experience for its author. Dr. Moody and Dr. Shugart never shut their doors and were always willing to put their schedules on hold to provide thoughtful advising, keeping this research on track when at times it seemed to be straying. Dr. Palace was willing to do the same from hundreds of miles away, sharing his unique and instrumental crown delineation software while providing the guidance (over the course of hundreds of emails) to traverse the learning curve associated with learning a new programming language. Dr. Swap must also be commended for his willingness to endure so many hours of discussions as he helped shape this research from nothing. He was there at every point in the arduous process of developing, refining and implementing such a research endeavor, providing the encouragement and mentoring needed to make this an exciting reality. In addition to his selfless advising, he was also instrumental in

helping secure funding for this research. In all, a more supportive, selfless, knowledgeable and generous committee could have been assembled for the purposes of this research. The author will forever and happily remain indebted to them.

In addition to Dr. Swap's contributions, this research was funded through the support of the Department of Environmental Science at the University of Virginia, the Virginia Space Grant Consortium, and the Eastern and Southern Africa and Virginia Networks and Associations (ESAVANA) Consortium.

7 Bibliography

Achard, F., Eva, H. D., Stibig, H.-J., Mayaux, P., Gallego, J., Richards, T., et al. (2002).

Determination of Deforestation Rates of the World's Humid Tropical Forests. *Science* , 999-1002.

Adams, J. B., & Gillespie, A. R. (2006). *Remote Sensing of Landscapes with Spectral Images: A Physical Modeling Approach*. Cambridge, United Kingdom: Cambridge University Press.

ARD, Inc. (2002). *Mozambique: Environmental Threats and Opportunities*. Burlington, VT: United States Agency for International Development.

Asner, G. P., Palace, M., Keller, M., Pereira, R. J., Silva, J. N., & Zweede, J. C. (2002).

Estimating Canopy Structure in an Amazon Forest from Laser Range Finder and IKONOS Satellite Observations. *Biotropica* , 483-492.

Asner, G. (2009). Tropical forest carbon assessments: integrating satellite and airborne mapping approaches. *Environmental Research Letters* , 1-11.

Basuki, T. M., van Laake, P. E., Skidmore, A. K., & Hussin, Y. A. (2009). Allometric equations for estimating the above-ground biomass in tropical lowland Dipterocarp forests. *Forest Ecology and Management* , 1684-1694.

Boucher, D., Elias, P., Lininger, K., May-Tobin, C., Roquemore, S., & Saxon, E. (2011). *The root of the problem: what's driving tropical deforestation today?* . Cambridge, MA: Union of Concerned Scientists.

Brandtberg, T., & Walter, F. (1998). Automated delineation of individual tree crowns in high spatial resolution aerial images by multiple-scale analysis. *Machine Vision and Applications* , 64-73.

- Broadbent, E. N., Asner, G. P., Pena-Claros, M., Palace, M., & Soriano, M. (2008). Spatial partitioning of biomass and diversity in a lowland Bolivian forest: Linking field and remote sensing measurements. *Forest Ecology and Management* , 2602-2612.
- Brown, S. (1997). *Estimating Biomass and Biomass Change of Tropical Forests: a Primer*. Rome: Food and Agriculture Organization of the United Nations.
- Burba, G., & Anderson, D. (2010). *A Brief Practical Guide to Eddy Covariance Flux Measurements*. Lincoln, NE: LI-COR Biosciences.
- Campbell, B. (1996). *The Miombo in Transition: Woodlands and Welfare in Africa*. Bogor, Indonesia: Center for International Forestry Research.
- Casper, B. B., Schenk, H. J., & Jackson, R. B. (2003). Defining a Plant's Below Ground Zone of Influence. *Ecology* , 2313-2321.
- Chambers, J. Q., Asner, G. P., Morton, D. C., Anderson, L. O., Saatchi, S. S., Espirito-Santo, F. D., et al. (2007). Regional ecosystem structure and function: ecological insights from remote sensing of tropical forests. *Trends in Ecology and Evolution* , 414-422.
- Chave, J., Andalo, C., Brown, S., Cairns, M. A., Chambers, J. Q., Eamus, D., et al. (2005). Tree allometry and improved estimation of carbon stocks and balance in tropical forests. *Oecologia* , 87-99.
- Chave, J., Condit, R., Aguilar, S., Hernandez, A., Lao, S., & Perez, R. (2001). Error propagation and scaling for tropical forest biomass estimates. *Philosophical Transactions of the Royal Society Biological Sciences* , 409-420.
- Choi, S., Ni, X., Shi, Y., Ganguly, S., Zhang, G., Duang, H. V., et al. (2013). Allometric Scaling and Resource Limitations Model of Tree Heights: Part 2. Site Based Testing of the Model. *Remote Sensing* , 202-223.

- Chubey, M. S., Franklin, S. E., & Wulder, M. A. (2006). Object-based Analysis of Ikonos-2 Imagery for Extraction of Forest Inventory Parameters. *Photogrammetric Engineering and Remote Sensing* , 383-394.
- Cohen, W. B., Maersperger, T. K., Gower, S. T., & Turner, D. P. (2001). An improved strategy for regression of biophysical variables and Landsat ETM+ data. *Remote Sensing of Environment* , 561-571.
- Committee on Earth Science and Applications from Space: A Community Assessment and Strategy for the Future. (2007). *Earth Science and Applications from Space: National Imperatives for the Next Decade and Beyond*. Washington, DC: National Academies Press.
- Corbera, E., Estrada, M., & Brown, K. (2010). Reducing greenhouse gas emissions from deforestation and forest degradation in developing countries: revisiting the assumptions. *Climatic Change* , 355-388.
- Culvenor, D. S. (2002). TIDA: an algorithm for the delineation of tree crowns in high spatial resolution remotely sensed imagery. *Computers and Geosciences* , 33-44.
- Defibaugh y Chavez, J., & Tullis, J. A. (2012). Deciduous Forest Structure Estimated with LIDAR-Optimized Spectral Remote Sensing. *Remote Sensing* , 155-182.
- DeFries, R. S., & Chang, J. C.-W. (2000). Multiple Criteria for Evaluating Machine Learning Algorithms for Land Cover Classification from Satellite Data. *Remote Sensing of Environment* , 503-515.
- DeFries, R. S., Rudel, T., Uriarte, M., & Hansen, M. (2010). Deforestation driven by urban population growth and agricultural trade in the twenty-first century. *Nature Geoscience* , 178-182.

- Dengsheng, L., & Batistella, M. (2005). Exploring TM Image Texture and its Relationships with Biomass Estimation in Rondônia, Brazilian Amazon. *ACTA Amazonica* , 249-257.
- Environmental Investigation Agency. (2013). *Mozambique loses a fortune to illegal timber exports*. London: Environmental Investigation Agency.
- FAO Subregional Office for Southern and East Africa, Harare. (2004). *Drought impact mitigation and prevention in the Limpopo River Basin* . Rome: Food and Agriculture Organization of the United Nations.
- Feldpausch, T. R., Banin, L., Phillips, O. L., Baker, T. R., Lewis, S. L., Quesada, C. A., et al. (2011). Height-diameter allometry of tropical forest trees. *Biogeosciences* , 1081-1106.
- Fensholt, R., Rasmussen, K., Nielsen, T. T., & Mbow, C. (2009). Evaluation of earth observation based long term vegetation trends - Intercomparing NDVI time series trend analysis consistency of Sahel from AVHRR GIMMS, Terra MODIS and SPOT VGT data. *Remote Sensing of Environment* , 1886-1898.
- Field, C. B., Randerson, J. T., & Malmstrom, C. M. (1995). Global Net Primary Production: Combining Ecology and Remote Sensing. *Remote Sensing of Environment* , 74-88.
- Food and Agriculture Organization of the United Nations, United Nations Development Program, United Nations Environment Programme. (2008). *UN Collaborative Programme on Reducing Emissions from Deforestation and Forest Degradation in Developing Countries (UN-REDD)*. New York City: United Nations.
- Foody, G. M. (2002). Status of land cover classification accuracy assessment. *Remote Sensing of Environment* , 185-201.

- Foody, G. M., Boyd, D. S., & Cutler, M. E. (2003). Predictive relations of tropical forest biomass from Landsat TM data and their transferability between regions. *Remote Sensing of Environment* , 463-474.
- Foody, G. M., Cutler, M. E., McMorrow, J., Pelz, D., Tangki, H., Body, D. S., et al. (2001). Mapping the biomass of Bornean tropical rain forest from remotely sensed data. *Global Ecology and Biogeography* , 379-387.
- Forster, P. V. (2007). *Changes in Atmospheric Constituents and in Radiative Forcing*. In: *Climate Change 2007: The Physical Science Basis. Contribution of Working Group I to the Fourth Assessment Report of the Intergovernmental Panel on Climate Change*. Cambridge: Cambridge University Press.
- Fortin, J. (2013, February 8). As China Imports Timber Illegally, Mozambique Pays the Price. *International Business Times* .
- Friedmann, H., & McNair, A. (2008). Whose Rules Rule? Contested Projects to Certify 'Local Production for Distant Consumers'. *Journal of Agrarian Change* , 408-434.
- Frolking, S., Palace, M. W., Clark, D. B., Chambers, J. Q., Shugart, H. H., & Hurtt, G. C. (2009). Forest disturbance and recovery: A general review in the context of spaceborne remote sensing of impacts on aboveground biomass and canopy structure. *Journal of Geophysical Research* , 1-27.
- FSC Forest Stewardship Council. (n.d.). *FSC Certification Database*. Retrieved 2013 йил 25-01 from Forest Stewardship Council: <http://info.fsc.org/>
- Geist, H. J., & Lambin, E. F. (2002). Proximate Causes and Underlying Driving Forces of Tropical Deforestation. *BioScience* , 143-150.

- Gibbs, H. K., Brown, S., Niles, J. O., & Foley, J. A. (2007). Monitoring and estimating tropical forest carbon stocks: making REDD a reality. *Environmental Research Letters* , 1-13.
- Gonzalez, P., Asner, G. P., Battles, J. J., Lefsky, M. A., Waring, K. M., & Palace, M. (2010). Forest carbon densities and uncertainties from Lidar, QuickBird, and field measurements in California. *Remote Sensing of Environment* , 1561-1575.
- Gordon, A., Tam, S., Bosquet, B., & R, A. A. (2011). *Forest Carbon Partnership Facility*. Washington, DC: World Health Organization.
- Governors' Climate and Forests Task Force. (2009). *Governors' Climate and Forests Task Force Joint Action Plan (2009-2010)*. Palo Alto, CA: Gordon and Betty Moore Foundation.
- Grainger, A. (2008). Difficulties in tracking the long-term global trend in tropical forest area. *Proceedings of the National Academy of Sciences* , 818-823.
- Hansen, M. C., Stehman, S. V., & Potapov, P. V. (2010). Quantification of global gross forest cover loss. *Proceedings of the National Academy of Sciences* , 8650-8655.
- Hansen, M. C., Stehman, S. V., Potapov, P. V., Loveland, T. R., Townshend, J. R., DeFries, R. S., et al. (2008). Humid tropical forest clearing from 2000 to 2005 quantified by using multitemporal and multiresolution remotely sensed data. *Proceedings of the National Academy of Sciences* , 9439-9444.
- Hely, C., Caylor, K., Alleaume, S., Swap, R. J., & Shugart, H. H. (2003). Release of gaseous and particulate carbonaceous compounds from biomass burning during the SAFARI 2000 dry season field campaign. *Journal of Geophysical Research* , 1-10.
- Henry, M., Picard, N., Trotta, C., Manlay, R. J., Valentini, R., Bernoux, M., et al. (2011). Estimating Tree Biomass of Sub-Saharan African Forests: a Review of Available Allometric Equations. *Silva Fennica* , 477-569.

- Houghton, R. A. (2003). Revised estimates of the annual net flux of carbon to the atmosphere from changes in land use and land management 1850-2000. *Tellus* , 378-390.
- Hurt, G., Xiao, X., Keller, M., Palace, M., Asner, G. P., Braswell, R., et al. (2003). IKONOS imagery for the Large Scale Biosphere-Atmosphere Experiment in Amazonia (LBA). *Remote Sensing of Environment* , 111-127.
- Ingram, J. C., Dawson, T. P., & Whittaker, R. J. (2004). Mapping tropical forest structure in southeastern Madagascar using remote sensing and artificial neural networks. *Remote Sensing of Environment* , 491-507.
- Keller, M., Palace, M., & Hurt, G. (2001). Biomass estimation in the Tapajos National Forest, Brazil: Examination of sampling and allometric uncertainties. *Forest Ecology and Management* , 371-382.
- Kuhlbusch, T. A., Andreae, M. O., Cahier, H., Goldammer, J. G., Lacaux, J.-P., Shea, R., et al. (2012). Black carbon formation by savanna fires: Measurements and implications for the global carbon cycle. *Journal of Geophysical Research* , 1-15.
- Le Quere, C., Raupach, M. R., Canadell, J. G., Marland, G., Bopp, L., Ciais, P., et al. (2009). Trends in the sources and sinks of carbon dioxide. *Nature Geoscience* , 1-6.
- Leckie, D. G., Gougeon, F. A., Tinis, S., Nelson, T., Burnett, C. N., & Paradine, D. (2005). Automated tree recognition in old growth conifer stands with high resolution digital imagery. *Remote Sensing of Environment* , 311-326.
- Lefsky, M. A., Cohen, W. B., Harding, D. J., Parker, G. G., Acker, S. A., & Gower, S. T. (2002). Lidar remote sensing of above-ground biomass in three biomes. *Global Ecology and Biogeography* , 393-399.

- Lim, K., Treitz, P., Wulder, M., St-Onge, B., & Flood, M. (2003). LiDAR remote sensing of forest structure. *Progress in Physical Geography* , 88-106.
- Lu, D. (2006). The potential and challenge of remote sensing-based biomass estimation. *International Journal of Remote Sensing* , 1297-1328.
- Macuacua, J. (2012). *Plan of Technical Cooperation with JICA under the REDD+ toward Formulation of REDD+ implementation Framework in Mozambique*. Maputo, Mozambique: Mozambique Department of Natural Resource Inventory.
- Miles, L., Newton, A., DeFries, R., Ravilious, C., May, I., Blyth, S., et al. (2006). A global overview of the conservation status of tropical dry forests. *Journal of Biogeography* , 491-505.
- Murphy, P. G., & Lugo, A. E. (1986). Structure and Biomass of a Subtropical Dry Forest in Puerto Rico. *Biotropica* , 89-96.
- Myeni, R. B. (1993). On the relationship between FAPAR and NDVI. *Remote Sensing of Environment* , 200-211.
- Nylan, R. D. (2002). *Silviculture: Concepts and applications*. Boston: McGraw Hill.
- Palace, M., Keller, M., Asner, G. P., Hagen, S., & Braswell, B. (2008). Amazon Forest Structure from IKONOS Satellite Data and the Automated Characterization of Forest Canopy Properties. *Biotropica* , 141-150.
- Palgrave, M. C., Van Wyk, A. E., Jordaan, M., White, J. A., & Sweet, P. (2007). A reconnaissance survey of the woody flora and vegetation of the Catapú logging concession, Cheringoma District, Mozambique. *Bothalia* , 57-73.

- Popescu, S. C., Wynne, R. H., & Nelson, R. F. (2003). Measuring individual tree crown diameter with lidar and assessing its influence on estimating forest volume and biomass. *Canadian Journal of Remote Sensing* , 564-577.
- Pouliot, D. A., King, D. J., Bell, F. W., & Pitt, D. G. (2002). Automated tree crown detection and delineation in high-resolution digital camera imagery of coniferous forest regeneration. *Remote Sensing of Environment* , 322-334.
- Ribeiro, N. S., Saatchi, S. S., Shugart, H. H., & Washington-Allen, R. A. (2008). Aboveground biomass and leaf area index (LAI) mapping for Niassa Reserve, northern Mozambique. *Journal of Geophysical Research* , 1-12.
- Ryan, C. M. (2009). *Carbon Cycling, Fire and Phenology in a Tropical Savanna Woodland in Nhambita, Mozambique*. Edinburgh, United Kingdom: University of Edinburgh.
- Saatchi, S. S., Houghton, R. A., Dos Santos Alvala, R. C., Soares, J. V., & Yu, Y. (2007). Distribution of aboveground live biomass in the Amazon basin. *Global Change Biology* , 816-837.
- Savcor Indufor Oy. (2005). *Actual Situation of the Forest Industry in Sofala, Zambezia and Cabo Delgado*. Maputo, Mozambique: Direcção Nacional de Terras e Florestas.
- Shugart, H. H., Bourgeau-Chavez, L., & Kasischke, E. S. (200). Determination of Stand Properties in Boreal and Temperate Forests Using High-Resolution Imagery. *Forest Science* , 478-486.
- Shugart, H. H., Saatchi, S., & Hall, F. G. (2010). Importance of structure and its measurement in quantifying function of forest ecosystems. *Journal of Geophysical Research* , 1-16.
- Spies, T. A. (1998). Forest structure: A key to the ecosystem. *Northwest Science* , 34-39.

- Toan, T. L., Quegan, S., Woodward, I., Lomas, M., Delbart, N., & Picard, G. (2004). Relating radar remote sensing of biomass to modelling of forest carbon budgets. *Climatic Change* , 379-402.
- Tomppo, E., Nilsson, M., Rosengren, M., Aalto, P., & Kennedy, P. (2002). Simultaneous use of Landsat-TM and IRS-1C WiFS data in estimating large area tree stem volume and aboveground biomass. *Remote Sensing of Environment* , 156-171.
- U.N., F. a. (n.d.). *Forest Cover Statistics for 2000*. Retrieved 2012 йил 19-January from Monga Bay: http://www.mongabay.com/forest_types_table.htm
- Umuntu Media. (2012). *Moçambique e Tanzania procuram travar exploração ilegal de recursos*. Maputo, Mozambique: iMozambique.
- Wild, H., & Barbosa, L. A. (1967). *Vegetation map of the Flora zambesiaca area*. Salisbury, Rhodesia: Collins.
- Wulder, M., Niemann, K. O., & Goodenough, D. G. (2000). Local Maximum Filtering for the Extraction of Tree Locations and Basal Area from High Spatial Resolution Imagery . *Remote Sensing of Environment* , 103-114.

8 Appendices

8.1 Appendix A

Selected relationships among the in-situ collected data.

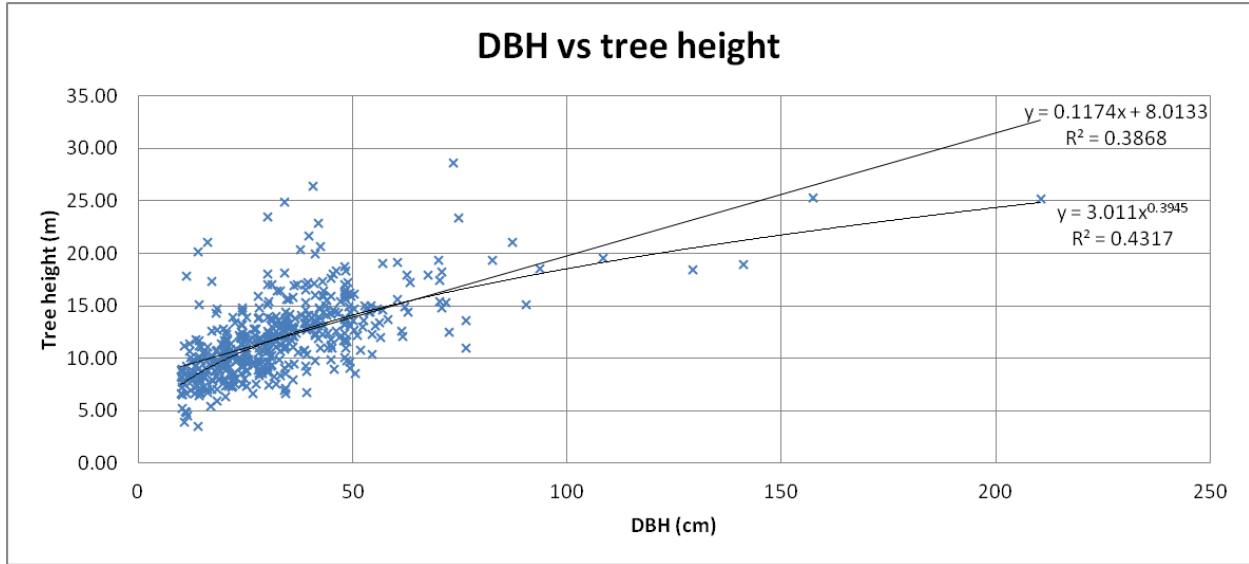


Figure 35: Relationship between DBH and tree height and its associated linear and power-based regressions.

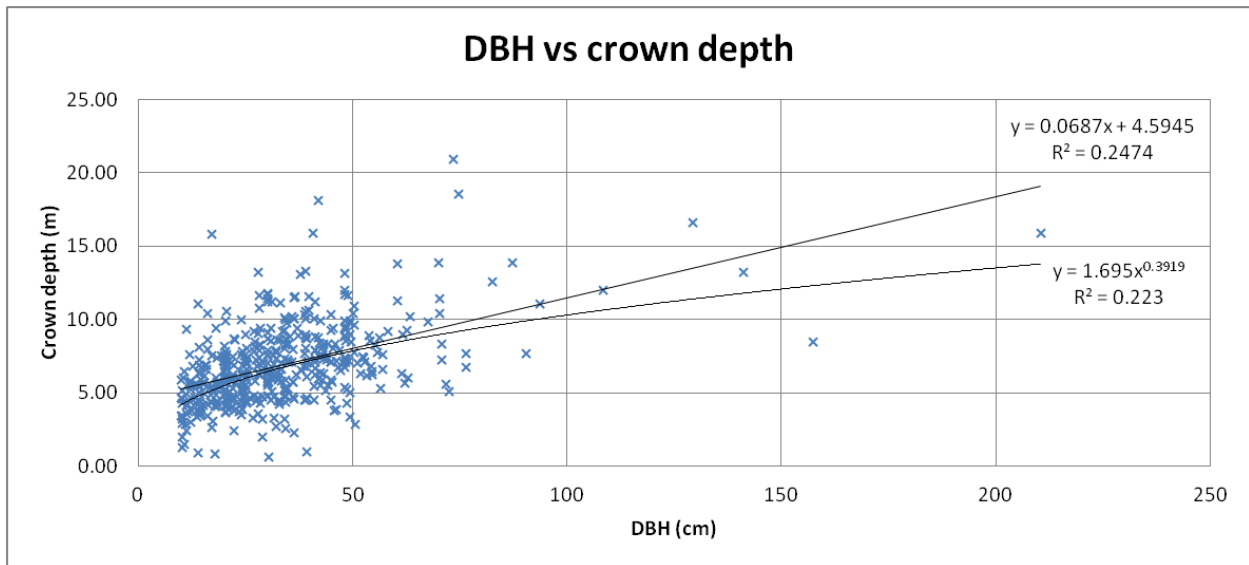


Figure 36: Relationship between DBH and tree crown depth and its associated linear and power-based regressions.

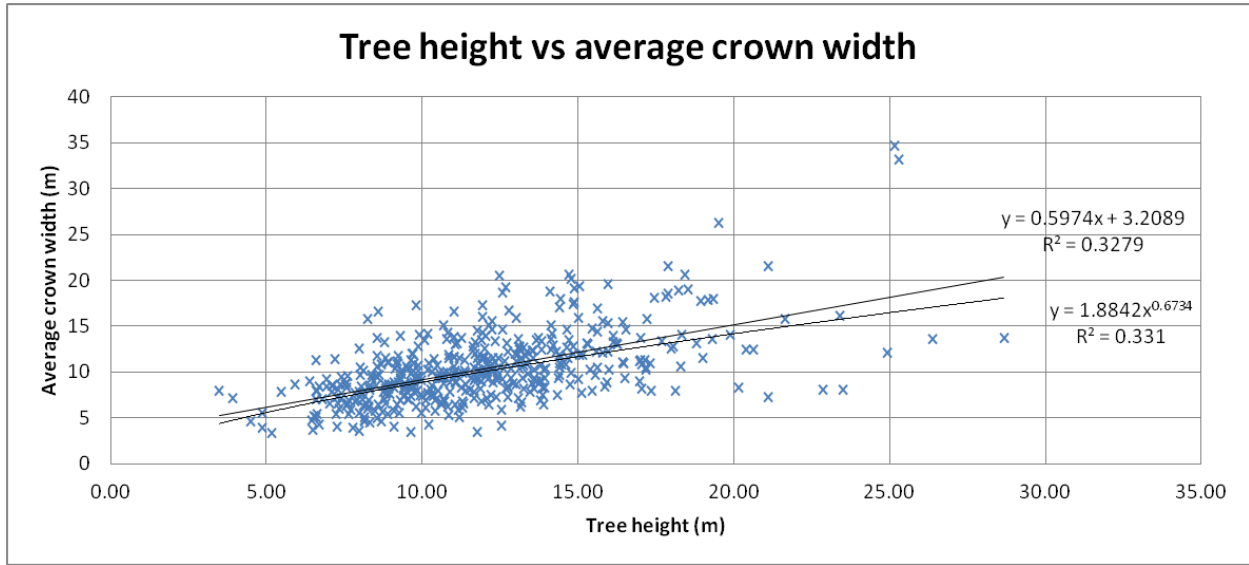


Figure 37: Relationship between tree height and average crown width and its associated linear and power-based regressions.

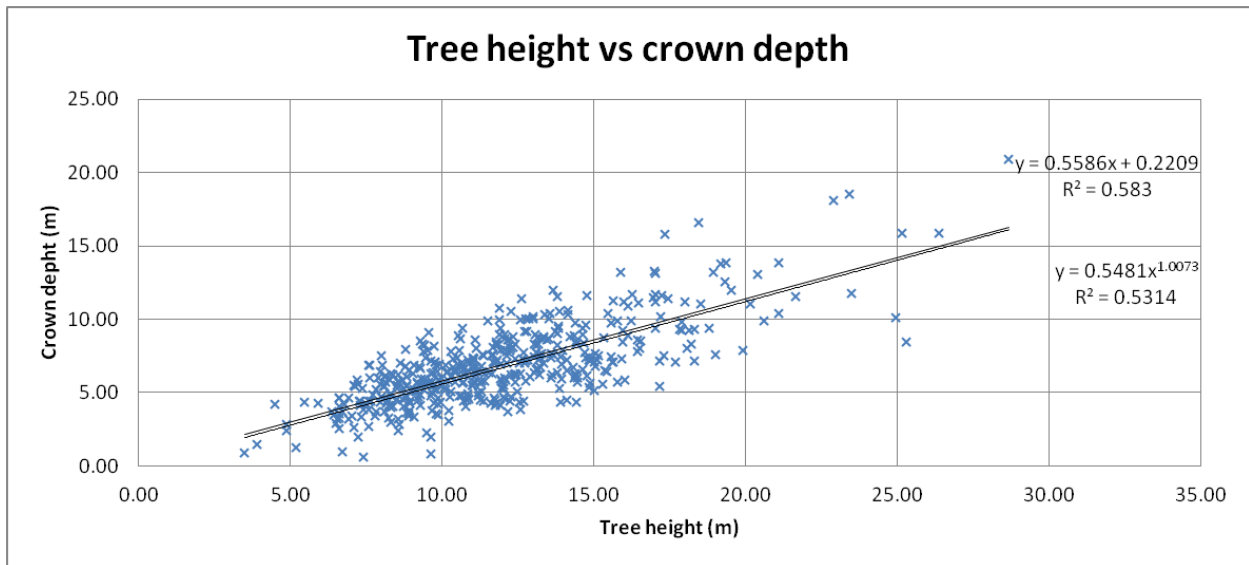


Figure 38: Relationship between tree height and tree crown depth and its associated linear and power-based regressions.

8.2 Appendix B

Comparative analysis based on stem densities and average tree diameter with the inclusion of intermediate forests.

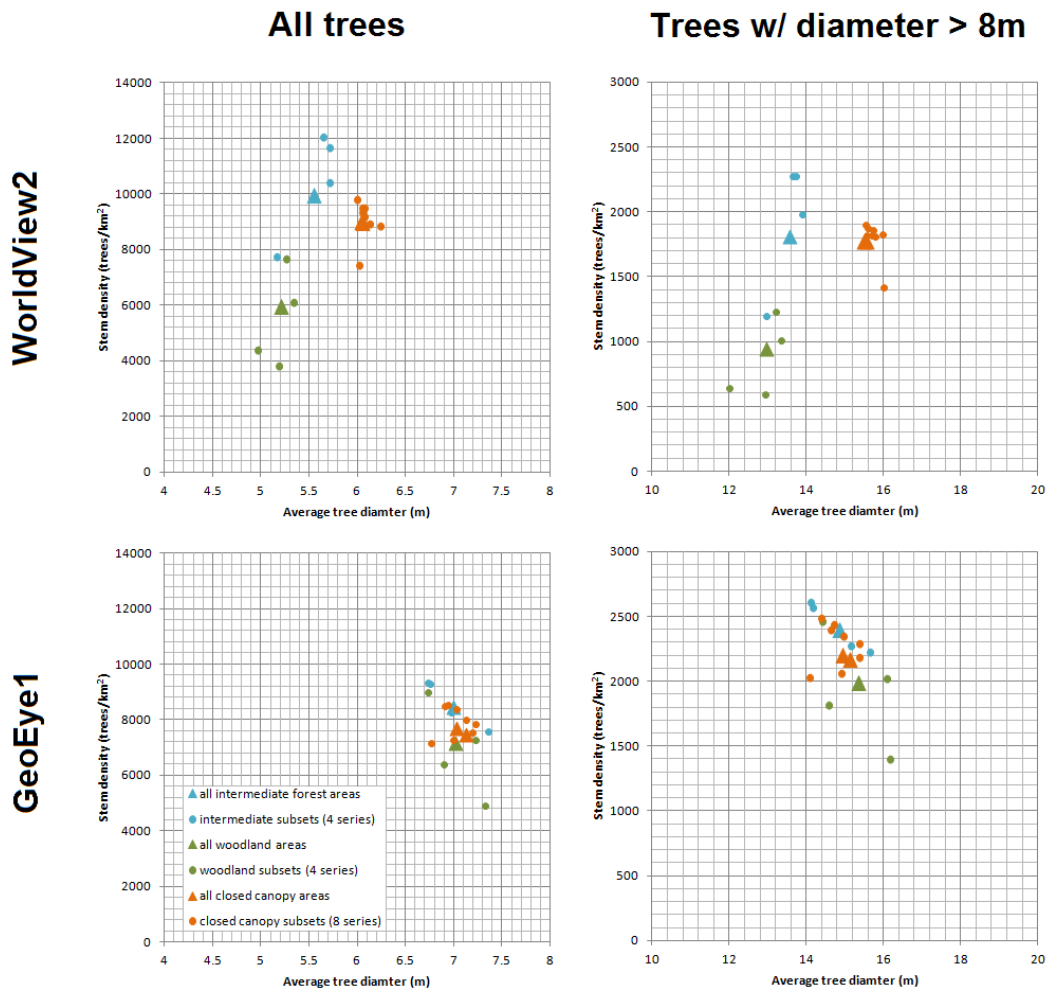


Figure 39: Scatter plots comparing average tree diameter and stem density for woodland (orange), intermediate semi-closed canopy (blue) and closed canopy (green) areas. Each subset is marked by a circle, while the aggregated sum for each type of forest is represented by a triangle (the two orange triangles represent each AOI). The four graphs additionally highlight the differences between WorldView2 and GeoEye1 analyses and due to the inclusion of an eight meter diameter threshold.

8.3 Appendix C

Illustrations of each AOI sub-dataset based on average diameter and stem density values.

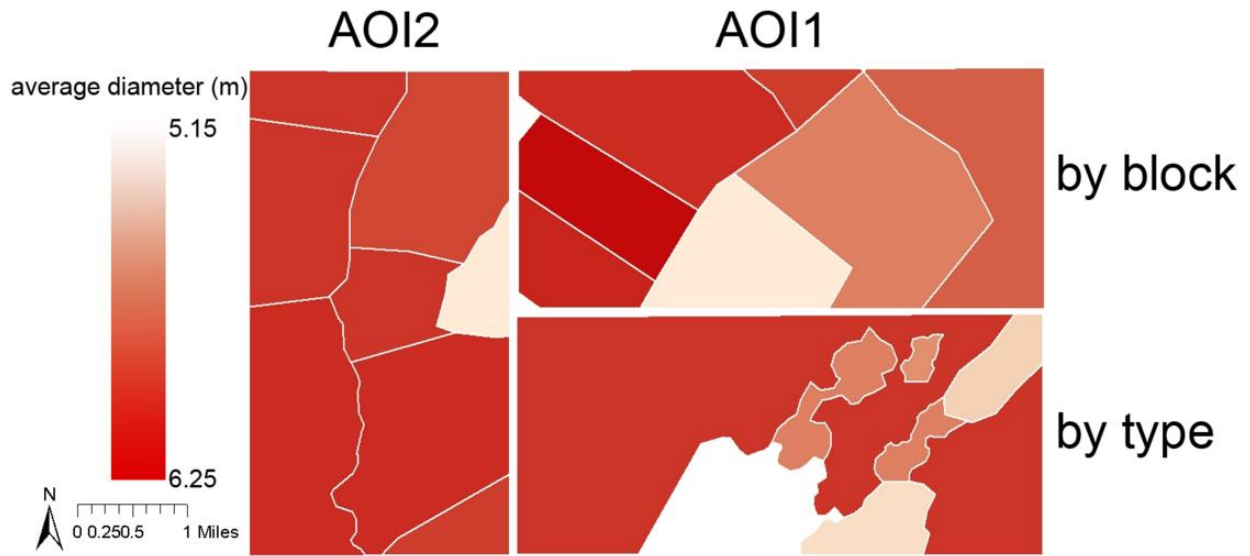


Figure 40: Geographic illustration of each sub-dataset in the WorldView2 analysis according to their mean diameter value. These values reflect the inclusion of all trees regardless of diameter.

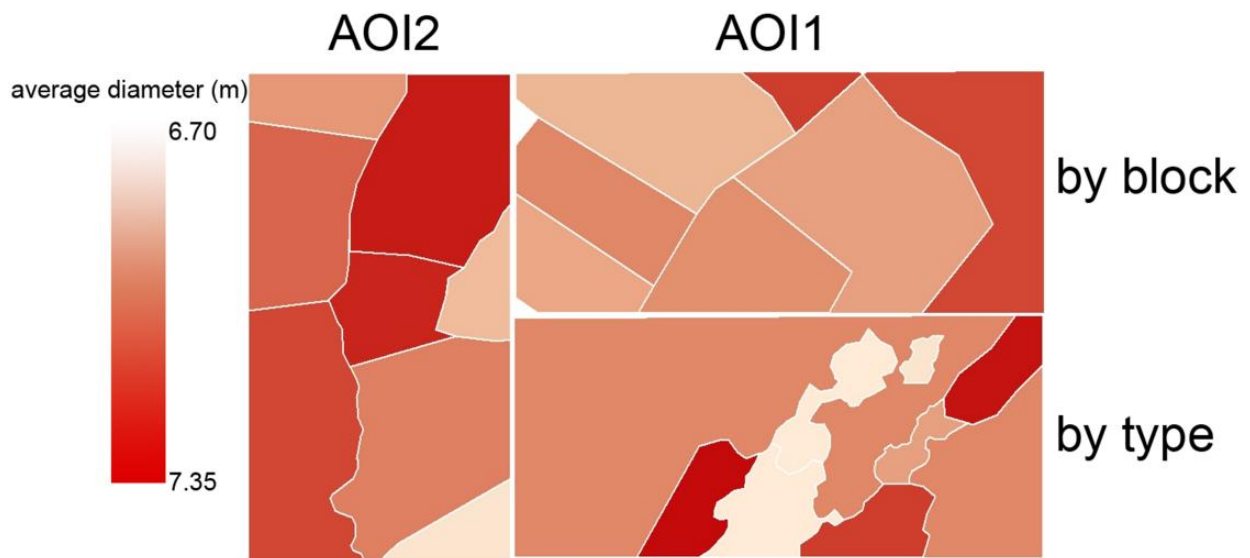


Figure 41: Geographic illustration of each sub-dataset in the GeoEye1 analysis according to their mean diameter value. These values reflect the inclusion of all trees regardless of diameter.

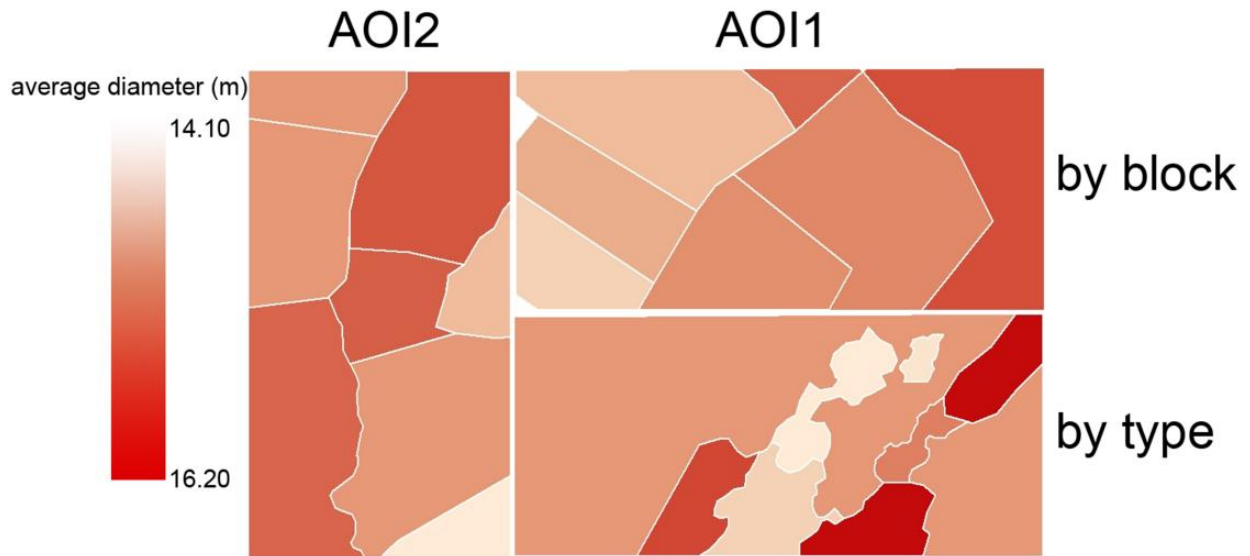


Figure 42: Geographic illustration of each sub-dataset in the GeoEye1 analysis according to their mean diameter value. These values reflect the inclusion of an eight meter diameter threshold.

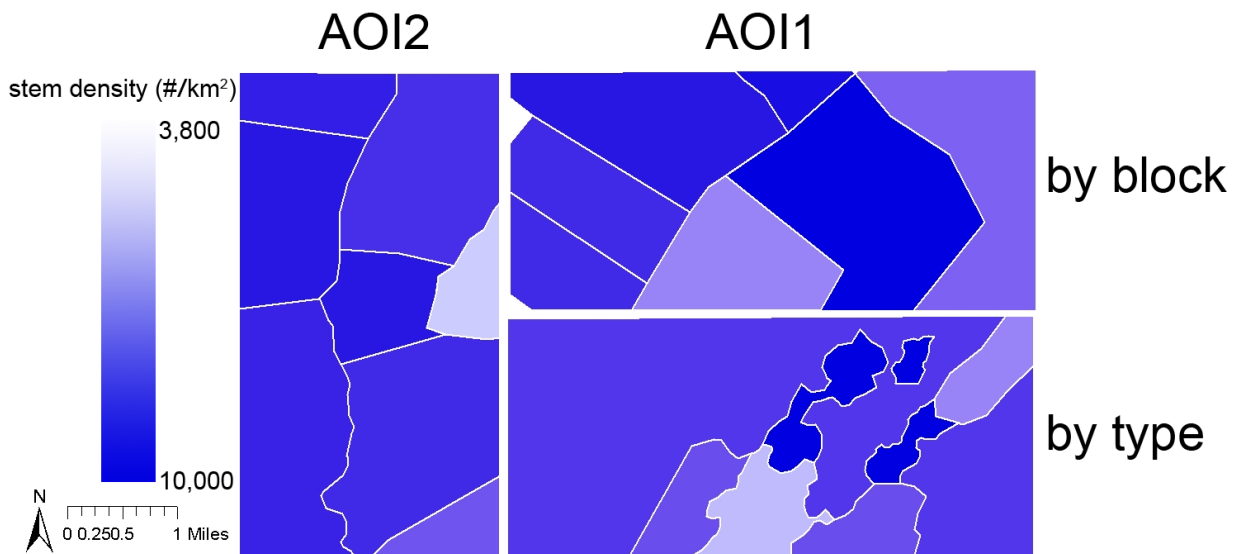


Figure 43: Geographic illustration of each sub-dataset in the WorldView2 analysis according to their stem densities. These values reflect the inclusion of all trees regardless of diameter.

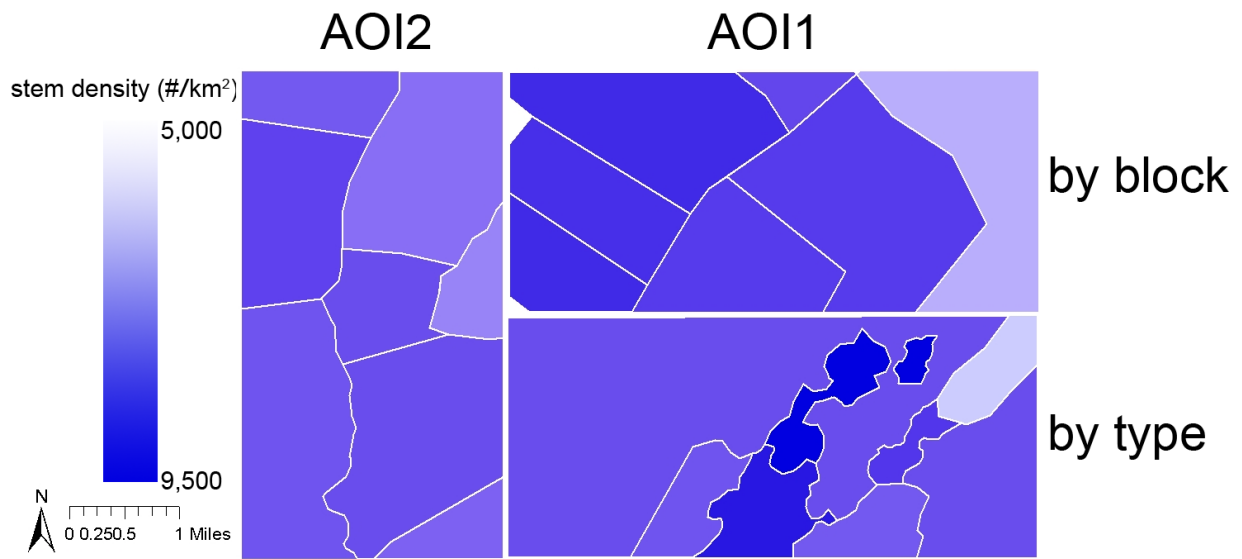


Figure 44: Geographic illustration of each sub-dataset in the GeoEye1 analysis according to their stem densities. These values reflect the inclusion of all trees regardless of diameter.

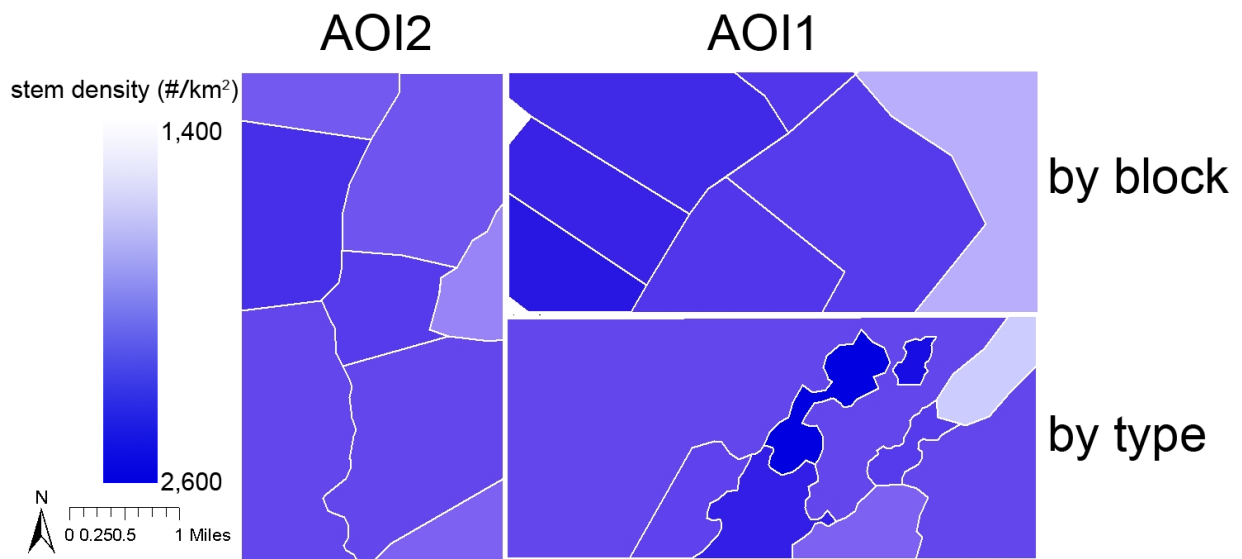


Figure 45: Geographic illustration of each sub-dataset in the GeoEye1 analysis according to their stem densities. These values reflect the inclusion of an eight meter diameter threshold.